N71-34283

NASA TECHNICAL NOTE NASA TN D-6487

NASA TN D-6487

TURBULENT MIXING OF COAXIAL COMPRESSIBLE HYDROGEN-AIR JETS

by James M. Eggers

Langley Research Center
Hampton, Va. 23365

NATIONAL AERONAUTICS AND SPACE ADMINISTRATION • WASHINGTON, D. C. • SEPTEMBER 1971

1. Report No.	2. Government Accession No.	3. Recipient's Catalog No.
NASA TN D-6487		

4. Title and Subtitle
TURBULENT MIXING OF COAXIAL COMPRESSIBLE HYDROGEN-AIR JETS

5. Report Date
September 1971

6. Performing Organization Code

7. Author(s)
James M. Eggers

8. Performing Organization Report No.
L-7901

9. Performing Organization Name and Address
NASA Langley Research Center
Hampton, Va. 23365

10. Work Unit No.
764-75-01-06

11. Contract or Grant No.

12. Sponsoring Agency Name and Address
National Aeronautics and Space Administration
Washington, D.C. 20546

13. Type of Report and Period Covered
Technical Note

14. Sponsoring Agency Code

15. Supplementary Notes

16. Abstract

An experimental and analytical study of the compressible turbulent mixing of parallel coaxial hydrogen-air jets has been conducted. Data were acquired for outer air jet Mach numbers of 1.32 and 2.50. The inner hydrogen jet Mach number was approximately 0.9 for both air jet Mach numbers. Experimental hydrogen mass fraction profiles and velocity profiles were determined throughout the near-field and far-field mixing regions. The validity of different eddy viscosity models was studied by incorporating them into an analysis and attempting to compute the present hydrogen-air data and previous air-air data. It was concluded that a kinematic formulation of eddy viscosity which provides radial as well as axial variation in dynamic eddy viscosity, through incorporation of the local density, is essential in order to compute both hydrogen-air and air-air mixing data.

17. Key Words (Suggested by Author(s))
Fluid mechanics
Turbulent mixing
Propulsion systems

18. Distribution Statement
Unclassified – Unlimited

19. Security Classif. (of this report)	20. Security Classif. (of this page)	21. No. of Pages	22. Price*
Unclassified	Unclassified	57	$3.00

*For sale by the National Technical Information Service, Springfield, Virginia 22151

TURBULENT MIXING OF COAXIAL COMPRESSIBLE

HYDROGEN-AIR JETS

By James M. Eggers
Langley Research Center

SUMMARY

An experimental and analytical study of the compressible turbulent mixing of parallel coaxial hydrogen-air jets has been conducted. Data were acquired for outer air jet Mach numbers of 1.32 and 2.50. The inner hydrogen jet Mach number was approximately 0.9 for both air jet Mach numbers. All jets had a total temperature near 300 K and mixed in an unconfined region at 1 atmosphere. Experimental hydrogen mass fraction profiles and velocity profiles were determined throughout the near-field and far-field mixing regions.

The validity of different eddy viscosity models was studied by incorporating them into a finite-difference-type analysis and attempting to compute the present hydrogen-air data and previous air-air data. A formulation of eddy viscosity based on a mass flow defect (or excess) across the mixing zone was unsatisfactory in computing the data. The kinematic eddy viscosity model of Cohen and a kinematic form of an eddy viscosity model used in a previous study both satisfactorily correlated the data. It was concluded that a kinematic form of eddy viscosity which provides radial as well as axial variation in dynamic eddy viscosity, through incorporation of the local density, is essential in order to compute both hydrogen-air and air-air mixing data.

INTRODUCTION

An interest in the computation of turbulent mixing exists because of the wide variety of applications. Typical problems involving turbulent mixing occur in jet-engine exhaust-noise generation, shear-layer interference heating, ejector design, mixing of pollutants with the atmosphere, and fuel injector design. The latter problem of fuel injector design, specifically the mixing of hydrogen fuel with air in a supersonic-combustion ramjet-engine combustor, is the motivation for this study. The study is restricted to consideration of the unconfined mixing of nonreactive, circular coaxial jets, which is an approximation to the downstream parallel injection of fuel from an in-stream injector.

In order to design a combustor for a hydrogen-fueled hypersonic ramjet engine, it is necessary to predict the fuel distribution obtained from a given injector design. For combustors of small height, it is conceivable to inject the fuel from the wall and achieve the desired uniform fuel distribution. As combustor size increases, however, it becomes necessary to consider injection from struts or, if the engine geometry permits, from an inlet center body in order to uniformly distribute the fuel. It is advantageous to inject the fuel in a downstream direction in order to benefit from the momentum of the fuel and in order to minimize pressure disturbances initiated by the fuel injection. Therefore, an analytical method is needed to predict the turbulent mixing of parallel compressible streams of hydrogen and air.

Unfortunately, current knowledge of the fundamental nature of turbulence is not sufficient to permit generation of a completely analytical solution to the mixing problem. Analysis of the mixing of turbulent flow fields has been performed by employing the boundary-layer equations with suitable models for the turbulence terms (conventional eddy viscosity and turbulent Prandtl and Lewis numbers). The semiempirical nature of the analysis arises through the need to specify the magnitude of the turbulent Prandtl and Lewis numbers and an eddy viscosity model. No universally accepted eddy viscosity model is currently available.

Many different eddy viscosity models have been proposed and reported in the literature. In reference 1, Ferri proposed a model relating the dynamic eddy viscosity to a mass flux difference. Later studies reported in reference 2 noted no tendency for two jets to remain segregated (unmixed) when the mass flux difference approached zero as Ferri's model would indicate. Also, no tendency was reported for two jets to remain unmixed when the velocity difference approached zero. From the studies of reference 2 it was not possible to determine whether the inadequacy of the Ferri model (or the inadequacy of Prandtl's model which expressed eddy viscosity as proportional to a velocity difference) was merely a limitation of the range of applicability of the models or an indication of invalidity. In reference 2, Alpinieri presented a model which was developed from purely empirical considerations and which correlated his data.

A more recent study by Schetz (ref. 3) expressed the dynamic eddy viscosity as being proportional to the mass flow defect (or excess) across the mixing zone. Also given in reference 3 were the computations resulting from using the Schetz model, the Prandtl velocity difference model, and the Ferri model. The general observation reported in the reference was that the Schetz model provided results in better agreement with the data considered than any other previously suggested model.

A kinematic eddy viscosity model has been developed by Cohen and reported in reference 4. The Cohen model was satisfactorily applied to hydrogen-air, hydrogen-nitrogen, reacting, and nonreacting data (ref. 5). Comparison calculations using the Prandtl velocity difference model, the Ferri model, and the Cohen model for high-temperature hydrogen-nitrogen mixing were also presented in reference 5. It was noted that the Prandtl model produced a much too slow mixing rate and the Ferri model produced a much too rapid mixing rate for the data considered.

Previous to the present study the author had participated in a coaxial air-air mixing study (ref. 6). Initial efforts to correlate the data were made with an eddy viscosity model attributed by the authors of reference 7 to Zakkay. It was found that limitations imposed by the definition of the mixing width in the Zakkay model restricted its application to the far-field mixing zone. Therefore, a new mixing width was defined and resulted in improved data correlation and a new dynamic eddy viscosity model.

Some additional eddy viscosity models for the region downstream of the potential core and wake flow have been summarized in reference 3. Despite the sizable number of mixing studies performed, illustrated by the numerous suggested eddy viscosity models, these have not resulted in guidelines which could be expected to lead to the development of a satisfactory eddy viscosity model. Progress in developing a satisfactory model has been hampered by the limited quantity of data each investigator has considered as well as the insufficiencies and uncertainties of the available data.

Data resulting from experiments involving nonreacting coaxial hydrogen-air mixing have been presented in references 1, 2, 5, 8, and 9. However, only references 1, 5, and 8 contain data where the airstream was supersonic, which is of primary interest for supersonic-combustion-ramjet application. Of these three references, only reference 5 (data referred to in ref. 5 are actually for hydrogen mixing with a high-temperature vitiated nitrogen stream) gives detailed survey data for the initial mixing conditions. Even in the data of reference 5, initial boundary layers are not well defined because the data were taken at an elevated temperature. As a result, the size of the total temperature probe limited the resolution of the data. The supersonic data of references 1 and 8 dealt only with the far field, that is, the flow field downstream of the potential core. It has been noted in reference 10 that the near field has received less attention than the far field although the near field is considered to be just as important in the overall design of a ramjet combustor. In summary, available supersonic hydrogen-air mixing data do not adequately define initial conditions or the near-field mixing region.

The purpose of the present investigation was twofold. The first objective was to generate detailed supersonic coaxial hydrogen-air mixing data, both in the near field and far field, which could be used to aid in the development of an analysis and eddy viscosity model. The second objective was to evaluate those eddy viscosity models available in the literature which were believed to offer the best chance of success in correlating the data. The eddy viscosity models chosen for this evaluation were those of Schetz (ref. 3) and Cohen (ref. 4) and that developed in a previously conducted air-air mixing study (ref. 6).

These three eddy viscosity models were incorporated into the analysis of reference 11. The validity of each model was determined by comparing analytical solutions to hydrogen-air data from the present study and air-air mixing data from reference 6. It was considered highly desirable that an eddy viscosity model permit the calculations to be initiated at the nozzle exit and to proceed continuously throughout the flow field. As eddy viscosity models are, in general, based upon dimensional analysis considerations, it was adjudged for this study that for the empirical constant to be truly a constant was too optimistic a viewpoint. Therefore, the value of the empirical constant associated with each model (assuming correct trends could be predicted) was chosen to best correlate the data.

Data were obtained corresponding to the nonreactive turbulent mixing of a circular coaxial near-sonic jet of hydrogen surrounded by a supersonic parallel stream of air at $M = 1.32$ or $M = 2.50$. The hydrogen jet Mach number was approximately 0.9 for both airstream Mach numbers. Representative unit Reynolds numbers are 1.18×10^6 per meter for the hydrogen jet and 3.71×10^6 per meter and 1.39×10^7 per meter for the Mach 1.32 and 2.50 air jets, respectively. The jets mixed in an unconfined region at a static pressure of 1 atmosphere (1 atm = 1.013×10^5 N/m^2). Both the hydrogen and air jets had total temperatures of approximately 300 K. Radial distributions of pitot pressure and hydrogen concentration were obtained downstream of the jet exit at various axial locations. These data were reduced to velocity and hydrogen mass fraction profiles and are tabulated in appendixes A and B.

SYMBOLS

A	area
b	a mixing-zone width defined as radial distance between points where velocities are u_3 and u_4
C_p	local specific heat at constant pressure
$C_{p,a}$	specific heat at constant pressure of pure air
$C_{p,h}$	specific heat at constant pressure of pure hydrogen
d	inner diameter of center nozzle, 11.6 mm
f^*	parameter in Cohen's eddy viscosity model (see eq. (8))
I	ratio of integrated hydrogen flow rate to metered hydrogen flow rate (see eq. (2))

k empirical constant for use with the Z-difference eddy viscosity model (see eq. (3))

k_2 empirical constant for use with the unified eddy viscosity model (see eq. (6))

k_3 empirical constant for use with the Cohen eddy viscosity model (see eqs. (8) and (9))

k_4 empirical constant for use with the kinematic Z-difference eddy viscosity model (see eq. (13))

L a characteristic length (see eq. (6))

M local Mach number

$\mathcal{M}$ local molecular weight

m ratio of outer jet velocity to center-line velocity, u_a/u_o

m_h metered center jet hydrogen flow rate

m_x integrated center jet hydrogen flow rate calculated from measured pressures, temperatures, and concentrations (see eq. (1))

m_1 velocity ratio fixed by turbulence level (see eq. (9))

N_{Le} turbulent Lewis number (the product of the turbulent diffusion coefficient and the constant-pressure specific heat divided by the turbulent thermal-conductivity coefficient)

N_{Pr} turbulent Prandtl number (the product of the constant-pressure specific heat and the turbulent viscosity divided by the turbulent thermal-conductivity coefficient)

N_{Sc} turbulent Schmidt number (ratio of turbulent Prandtl number to turbulent Lewis number)

n ratio of outer jet density to center-line density

n_1	density ratio fixed by turbulence level (see eq. (9))
p	static pressure
$\overline{R}$	universal gas constant
R	local gas constant
T	static temperature
T_t	total temperature
u	axial velocity, m/sec
u_1	velocity defined by equation (4)
u_2	velocity defined by equation (5)
u_3	velocity defined by equation (10)
u_4	velocity defined by equation (11)
x	axial coordinate
y	radial coordinate
z	a mixing-zone width defined as radial distance between points where velocities are u_1 and u_2
α	local mass fraction of hydrogen (local mass of hydrogen divided by sum of local mass of hydrogen and local mass of air)
β	local volume fraction of hydrogen
γ	ratio of specific heats
δ_*^2	a displacement thickness defined by equation (7)
ϵ_t	eddy viscosity in kinematic form

$(\rho\epsilon)_t$ dynamic eddy viscosity

ρ density

Subscripts:

a evaluated in external airstream (see fig. 3)

j evaluated in hydrogen flow at jet exit and on jet center line

o evaluated on center line

Bar over symbol indicates that parameter is nondimensionalized by the center nozzle external diameter (12.7 mm).

APPARATUS

Nozzle

A sketch of the nozzle configuration used to generate the flow fields of this study is shown in figure 1(a). Nozzle contours are given in figures 1(b), 1(c), and 1(d). A Mach 1.32 circular-contoured plug nozzle with a subsonic circular nozzle contained in the center body was used in the initial phase of this study. A second phase employed a Mach 2.50 circular-contoured plug nozzle with the subsonic circular center nozzle. The exit diameter for both plug nozzles was 15.2 cm. The subsonic nozzles had inner and outer exit diameters of 11.6 mm and 12.7 mm, respectively. (See enlarged sketch in fig. 1(a)). The flow passage in the subsonic nozzles converged slightly in the flow direction to ensure that if choking occurred it would occur at the nozzle exit. The taper was approximately 0.005 cm/cm on the diameter. The tapered section extended approximately 10 cm upstream of the nozzle exit at which point the internal diameter was increased to 25.4 mm; this enlarged diameter resulted in the flow area being increased by a factor of approximately 4.

An exhaust duct 76 cm in diameter was located approximately 1 m downstream of the nozzle exit and thus provided means of exhausting the hydrogen-air jets from the test area. The inlet to the test cell was open to the atmosphere and provided sufficient flow area to prevent any detectable decrease in static pressure in the test chamber during data acquisition.

Survey Rake

A remote controlled actuator was installed at various distances in the axial direction from the nozzle exit and was used to traverse a survey rake across the flow field. The rake position was indicated by a servodriven counter. The counter which indicated probe location was calibrated to be 195 counts/cm with an observed uncertainty of ±2 counts. The survey rake contained a pitot probe and a static-pressure probe which were 4.06 cm apart. Significant details of the rake and probes are shown in figure 2. A flow-field schematic is shown in figure 3.

Gas Analysis

Gas samples were piped directly from the rake to the injection valve in a gas chromatograph. Standard gas chromatography techniques similar to those described in reference 12 were used to perform the gas analysis. Briefly, this technique involves separation of the hydrogen from other gas components by passing the sample through a silica gel column followed by a molecular sieve column. The separated gas components then were passed through a thermistor detector. The output of this detector relative to that of a reference detector exposed to pure nitrogen carrier gas is an indication of the volume of hydrogen in a given sample. The detector output was recorded on a strip chart recorder. Comparison of the peak height output to peak heights corresponding to known mixtures of hydrogen and nitrogen gave the volume percent hydrogen in a sample. Pertinent data on the columns are as follows:

Column 1: silica gel; mesh 60/70; diameter, 3.18 mm; length, 122 cm; conditioned for 4 hr at 470 K with argon gas purge.

Column 2: molecular sieve; 5 Å; 70/80 mesh; diameter, 3.18 mm; length, 183 cm; conditioned for 6 hr at 620 K with argon purge.

The nitrogen carrier gas flow rate was approximately 45 standard cm^3/min. The columns were maintained at 310 K during gas analysis. Errors in gas analysis are not significant in comparison to the uncertainty of obtaining representative gas samples from the turbulent flow field.

TEST PROCEDURE

A constant flow of dry air at near-ambient temperature was supplied to the plug nozzle through a duct 36 cm in diameter. Ambient-temperature hydrogen was supplied to the inner nozzle through a support pipe. The temperature of each stream was measured in the supply pipes by use of iron-constantan thermocouples. For the established flow conditions, static-pressure orifices near the outer nozzle exit indicated ratios of nozzle-exit static pressure to atmospheric static pressure of 1.02 and 0.97 for the Mach

1.32 and Mach 2.50 jets, respectively. Radial surveys of pitot pressure and hydrogen concentration were performed at several axial stations in the flow field. A limited number of probe static-pressure surveys were also performed. Survey locations and temperatures for the two test conditions studied are summarized in table I. Schlieren photographs were also taken to aid in interpreting the data. Typical flash and time-exposure schlieren photographs are presented in figures 4 and 5.

During the early stages of the study, gas samples were extracted from the flow field through a pitot probe tip of the type shown in figure 2. Only the pitot pressure was used as the pumping force to extract these samples. In order to assess the accuracy of the data, the following integral was evaluated for each axial survey station:

$$m_x = \sqrt{\gamma} \int_A \frac{\alpha p M}{\sqrt{RT}} \, dA \tag{1}$$

Details on the evaluation of equation (1) are given in appendix C. The magnitude of m_x should be equal to the metered hydrogen flow rate m_h, or the magnitude of I as given by

$$I = \frac{m_x}{m_h} \tag{2}$$

should be near unity if there are no substantial errors in the data. Any deviation of I from unity is due to experimental error. For hydrogen-air mixing, I is particularly sensitive to hydrogen concentration. Typical values of I computed from the initial data were in the range of 0.7 to 0.8 which indicated that 20 to 30 percent of the hydrogen jet flow was not accounted for in the gas sample data. Attempts to obtain higher concentration values by aspirating the gas sample through the pitot probe and by pumping on the probe were unsuccessful inasmuch as no improvement was noted in the concentration data. A recent study (ref. 13) noted that differences between integrated and measured mass flows of 20 percent are considered typical.

The problem of obtaining representative gas samples has been discussed in reference 6. It was concluded in reference 6 that the actual physical mechanism which causes the sampling probe to obtain unrepresentative samples is not known; however, the results suggest that the erroneous concentration measurements are related to the local turbulence level in the flow field. It was noted in reference 14 that when sampling through a static probe, representative gas samples were always obtained. Therefore, several concentration surveys were performed with the Mach 1.3 static probe (fig. 2) and a diaphragm-type pump to extract the gas sample. A comparison of the gas concentration obtained by pitot probe sampling and static-pressure probe sampling is presented in figure 6 for two axial stations. It is evident from the data in figure 6 that significantly higher gas concentrations were obtained with the static probe sampling technique. Reduction of the static-pressure-probe sampling data of figure 6 resulted in ratios of integrated hydrogen flow rate to measured hydrogen flow rate (eq. (2)) very near unity. Due to this excellent agreement, the static probe tips shown in figure 2 were used to extract all gas samples in the remainder of this test program.

Some uncertainty in the axial location of the concentration data is introduced by sampling through the static probe. The uncertainty is due to the inability to positively determine whether the gas samples are representative of the flow at the probe tip or at the location of the static orifices. However, the boundary-layer flow on the probe will stabilize the small-scale turbulent flow field and thereby mixing is reduced in the vicinity of the probe surface. Thus, gas samples taken through the static orifices would be expected to have undergone less mixing than actually occurred in the undisturbed flow field. The concentration data are therefore expected to be representative of the flow field at some location ahead of the static orifice (but of course not ahead of the probe tip). For this study (including the data of fig. 6), the tip of the static probe was positioned at the same axial location as the tip of the pitot probe. The concentrations measured were assumed to be representative of the flow field and the axial location of the probe tip. A comparison of the dimensions of the static probes and the center nozzle diameter indicates that the concentration data may be displaced downstream from the pitot pressure survey by up to 1 jet diameter for the $M_a = 1.32$ data. Similarly, the concentration may be displaced up to 1.54 jet diameters from the pitot pressure survey for the $M_a = 2.50$ data. The actual error introduced depends upon the axial total-pressure gradient and concentration gradient at each particular survey station and the effect of the interaction between the probe and the flow field.

As an indication of the accuracy of the data, values of I from equation (2) have been listed in table I. As shown in table I(a), values of integrated hydrogen flow rate ranged from 16 percent low to 4 percent high for the $M_a = 1.32$ data. Poorer accuracy was achieved for the $M_a = 2.50$ data where integrated hydrogen flow rates ranged from 12 percent low to 29 percent high. It is noted that values of I greater than 100 percent were calculated in the region of the flow field where large gradients in pitot pressure and concentration existed (from $x/d = 4.31$ to $x/d = 15.36$).

DATA REDUCTION

The measured pitot pressures, total temperature, and volumetric concentration of hydrogen were reduced to velocity profiles and hydrogen mass fraction profiles. The method employed is identical to the technique used in evaluating equation (1). Specific equations are presented in appendix C. The center of the hydrogen concentration profiles was assumed to be the center of the flow field. An assumption of uniform static pressure equal to atmospheric pressure was used in all data reduction. Probe static-pressure measurements were found to be seriously affected by shock-wave intersections with the probe and were not used in data reduction.

It was observed during data reduction that the extent of the mixing zone (the region where hydrogen-air mixtures existed) could be determined from the fluctuations in the pitot-pressure signal. In the region of large gradients (in the mixing zone near the concentration potential core), pitot-pressure fluctuations were as high as ±7.1 percent in an extreme case. (These fluctuations are not to be taken as indicative of the actual magnitude of the turbulence of the flow as they are a function of the recording system employed, but the pitot-pressure fluctuations are an indication of large turbulent fluctuations in the mixing zone.) The fluctuation in pitot pressure decreased to an insignificant value as either the undisturbed hydrogen potential core flow or the undisturbed airflow was approached. Some evidence of large-scale mixing vortices, and thus associated fluctuations, may be seen in figures 4(a) and 5(a), as the mixing boundaries are irregular in the schlieren flash photographs. Mean values of pitot pressure from the strip chart record were used in data analysis. The local Mach number, mass fraction, and velocity data are tabulated in appendixes A and B.

Concentration values required to compute local velocities were read from plots of the radial distribution of concentration inasmuch as pitot-pressure and concentration measurements were not necessarily made at the same radial location.

THEORY

Analysis

The analysis of reference 11 was used to correlate the experimental data of this study and the air-air mixing data from reference 6. The analysis employs equilibrium chemistry, transformation techniques, and an explicit finite-difference technique to compute turbulent mixing and reacting of parallel streams of hydrogen and air. Axial pressure gradients and nonunity turbulent Prandtl and Lewis numbers are provided for in the analysis. The analysis is applicable to both the near and far field providing a proper eddy viscosity model is specified. Further details of the analysis are given in reference 11. Information on the use of the computerized analysis may be found in reference 7.

In order to analyze the hydrogen-air mixing data without allowing a reaction to occur, the airstream was simulated by pure nitrogen. For air-air mixing, the center jet was specified as an oxygen-nitrogen mixture corresponding to that of air (oxygen mass fraction 0.232, nitrogen mass fraction 0.768) and the outer stream as pure nitrogen. The oxygen thus defined the extent of mixing of the center jet. Specifying the concentration composition as just noted retains the validity of the mixing analysis by maintaining the approximately correct molecular weight ratio between the streams.

Eddy Viscosity Models

Different eddy viscosity models were incorporated in the analyses to test their validity. The first model examined herein was developed in reference 6 and is expressed as

$$(\rho\epsilon)_t = kz(\rho u)_o \tag{3}$$

In equation (3), $(\rho\epsilon)_t$ is the dynamic eddy viscosity, k is an empirical constant, and $(\rho u)_o$ is the mass flux per unit area on the jet center line. The mixing-zone width z is defined as the radial distance between the points where the local velocities are u_1 and u_2 as given by the following equations:

$$u_1 = u_a + 0.95(u_o - u_a) \tag{4}$$

$$u_2 = u_a + 0.50(u_o - u_a) \tag{5}$$

The definitions of u_1, u_2, and z are illustrated in the following sketch:

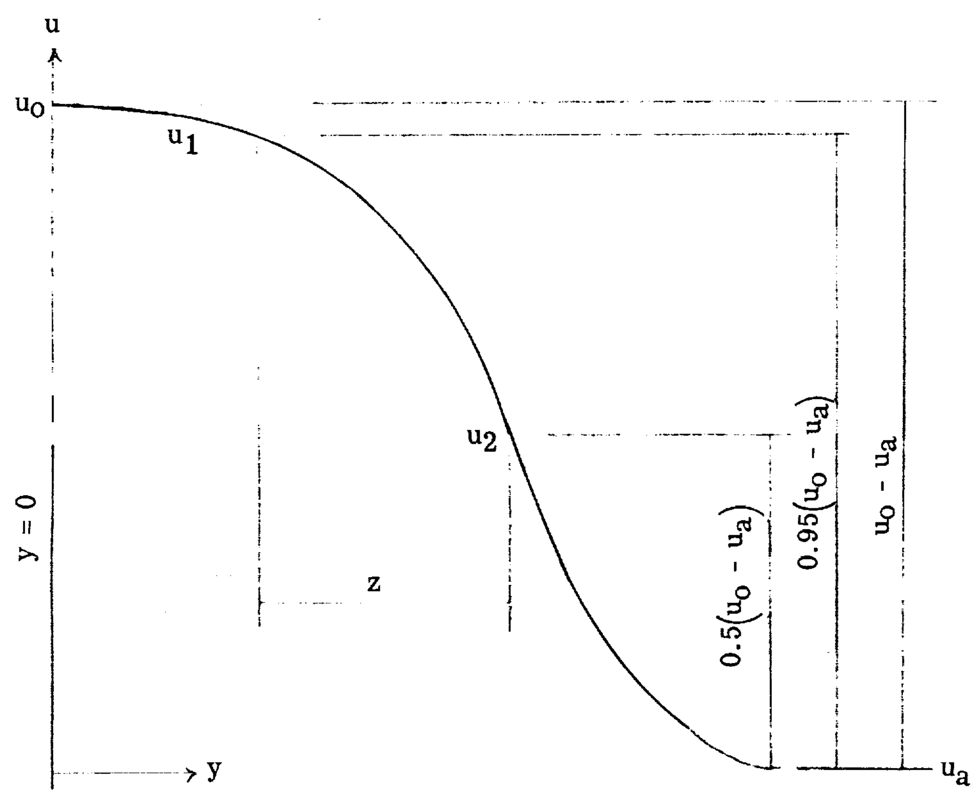

The eddy viscosity model of equation (3) is hereinafter referred to as the Z-difference model and was satisfactorily used in reference 6 to correlate air-air mixing data. Values of k employed in reference 6 were of the order of 0.01 and varied slightly with test conditions.

The second model considered relates the eddy viscosity to the mass flow defect (or excess) across the mixing zone. This model was termed the "unified" eddy viscosity model in reference 3 and is given by

$$(\rho\epsilon)_t = \frac{\pi k_2 (\rho u)_a \delta_*^2}{L} \tag{6}$$

In equation (6), πk_2 is an empirical constant, $(\rho u)_a$ is the mass flow per unit area in the outer stream, and L is a characteristic length assumed to be the nozzle radius. The displacement thickness δ_*^2 is expressed as

$$\delta_*^2 = 2\int_0^\infty \left|1 - \frac{\rho u}{(\rho u)_a}\right| y\,dy \tag{7}$$

Correlation of data using the unified model of equation (6) was reported in reference 3 by using a value of πk_2 of 0.018. In the context of the usage of equation (6) in reference 3, the constant πk_2 was unchanged which implies that the constant is independent of test conditions and applicable to all data. A limitation in equation (6) is that defining the characteristic length L as the nozzle radius is a very poor approximation in the region near the nozzle exit. Therefore, the application of equation (6) is expected to be confined to the downstream region of the flow field.

The third eddy viscosity model considered was developed in reference 4 and is hereinafter referred to as the Cohen viscosity model. It differs from the other two models by employing the kinematic eddy viscosity. The model is defined by the following equations:

$$\epsilon_t = k_3\left(f^* \frac{\rho_o + \rho_a}{2\rho_o}\right)^{0.8} b\left(u_o - u_a\right) \tag{8}$$

$$\epsilon_t = k_3\left(\frac{1 + n_1}{2}\right)^{0.8} b\left|1 - m_1\right| u_o \frac{\left(1 + n_1\right)(1 + mn)}{(1 + n)\left(1 + m_1 n_1\right)} \tag{9}$$

In equations (8) and (9), k_3 is an empirical constant, f^* is an empirical parameter equal to unity for incompressible mixing but which may vary with Mach number, ρ_o is the density on the jet center line, ρ_a is the density in the external flow, u_o is the velocity on the jet center line, and u_a is the velocity in the external flow. In equations (8) and (9), the mixing-zone width b is defined as the distance across the mixing zone between the points where the velocities are u_3 and u_4 as given by the following equations:

$$u_3 = u_a + 0.95(u_o - u_a) \tag{10}$$

$$u_4 = u_a + 0.05(u_o - u_a) \tag{11}$$

In equation (9), n is the density ratio ρ_a/ρ_o, m is the velocity ratio u_a/u_o, n_1 is a density ratio fixed by turbulence level, and m_1 is a velocity ratio fixed by turbulence level. Equation (8) is to be used if $m \leqq m_1$, and equation (9) is to be used for $m > m_1$. The value of n_1 is to be calculated at the axial station where $m = m_1$. If the initial velocity ratio exceeds m_1, n_1 is to be taken as the ratio of the external stream density to the initial jet density. In reference 4, f^* was taken as unity and m_1 was taken equal to 0.40. A value of k_3 of 0.00764 was suggested for the core region and a somewhat larger value of 0.0089, for the downstream region. As it did not appear possible to change the value of the constant k_3 between the near field and the far field without introducing discontinuities, a constant value of k_3 was used throughout the flow field for all computations presented herein. Note that the dynamic eddy viscosity $(\rho\epsilon)_t$, obtained from the local density and equations (8) and (9), varies in both the radial and axial directions. The other two eddy viscosity models as given by equations (3) and (6) permit eddy viscosity variations in only the axial direction.

DATA PRESENTATION AND CORRELATION

General Comments

It is recognized that a transition region exists between the quasi-two-dimensional near-field mixing region and the far-field fully developed profiles. However, turbulent flow theory is not sufficiently developed to provide a means of treating this transition region. Therefore, in this study, as has been the approach of most investigators (see ref. 3 for further discussion on the neglect of the transition region), the flow field is considered to consist of only a near-field mixing region and a far-field mixing region (fig. 3). The neglect and inadequate knowledge of how to treat the transition region result in poorer data correlation in the region near the end of potential core than in the remainder of the flow field, as evidenced by the results of reference 6 and of this study. This inaccuracy has been accepted in order to provide an eddy viscosity model which permits initiation of calculations at the nozzle exit and which permits continuous calculations to proceed throughout the flow field.

A primary purpose of this study was to evaluate several eddy viscosity models. It was realized that limiting the theoretical calculations to the two sets of hydrogen-air mixing data generated in this study was too restrictive an evaluation. Therefore, air-air mixing data from reference 6 was included in this study to evaluate the three eddy viscosity models of interest.

A technique of evaluating a particular eddy viscosity model is to compare experimental center-line velocity distributions with those predicted by a particular model and a selected value of the empirical constant. Once the empirical constant is selected, it remains to determine the best values of the turbulent Lewis number N_{Le} and turbulent Prandtl number N_{Pr} to correlate the center-line mass fraction distribution. It is important to remember that any eddy viscosity model can be made to fit a particular center-line velocity data point by a judicious choice of the empirical constant. However, the remainder of the data distribution will not necessarily be correlated. It was found in a previous study (ref. 6) that if the center-line velocity and concentration axial distributions were reasonably well correlated, then the radial profiles were also reasonably correlated. Therefore, the center-line correlation technique was used to evaluate eddy viscosity models in this study. Center-line velocity data from the current hydrogen-air mixing study and from the air-air mixing study of reference 6 are first presented. Presentation of radial velocity profiles and center-line and radial distributions of hydrogen mass fraction from the hydrogen-air mixing data are deferred until the eddy viscosity models are evaluated.

Hydrogen-Air Velocity Data

$\underline{M_a = 1.32}$.- The center-line velocity data for $M_a = 1.32$ and $M_j = 0.89$ are presented in figure 7(a). It is noted that the center-line velocity decays in a consistent manner and approaches the free-stream velocity at the most downstream station ($x/d = 63.6$). Integrated mass flows as previously discussed and given in table I give a good degree of confidence in the reliability of these data. It was noted during data reduction that the data for $x/d = 0$ were for a higher hydrogen jet total temperature than the remainder of the data. Therefore, the total temperature (and thus the velocity) in the hydrogen jet was reduced to a value representative of the entire data set before initiating theoretical calculations.

$\underline{M_a = 2.50}$.- The center-line velocity data for $M_a = 2.50$ and $M_j = 0.91$ are presented in figure 7(b). For $x/d = 4.31$, 8.75, and 15.36 integrated mass flows averaged 27 percent high. (See table I.) It is believed that the high values resulted from uncertain concentration measurements in the region of large radial gradients where large fluctuations occur. The accuracy of the data at the downstream stations ($x/d = 19.8$ to 58.0) is believed to be good inasmuch as integrated mass flows of 0.88 to 0.96 were calculated.

The data show an unexpected decrease in center-line velocity to values below the free-stream velocity for values of x/d near 20 and larger. Calculations indicate that the concentration measured near the center line at $x/d = 19.8$ would have to be increased 13.6 percent in order to increase the computed center-line velocity to the magnitude of the free-stream velocity. Uncertainties in the concentration measurements are not believed large enough to explain the below free-stream velocity values. Center-line velocity data at stations beyond $x/d = 19.8$ are less sensitive to the concentration measurements due to the low magnitude of the concentration.

The unexpected low center-line velocities may be explained in terms of the relative rates of mass and momentum transfer. The fact that mass transfer is faster than momentum transfer has been established experimentally (turbulent Schmidt number less than 1 for similar profiles). Therefore, the velocity can decrease axially even though the Mach number is increasing, as was found for the Mach 1.32 hydrogen-air velocity distribution. If the mass transfer is rapid enough relative to the momentum transfer, then a decrease in center-line velocity below free-stream velocity can occur as exemplified by the Mach 2.50 data. The difference in trends between the Mach 2.50 and Mach 1.32 center-line velocity data may be explained by noting that there was a smaller difference between jet and free-stream velocities for the Mach 2.50 data. Therefore, relatively less rapid momentum transfer would occur and the mass transfer effect would be more predominant than in the Mach 1.32 hydrogen-air mixing data.

A complex pattern of shock waves is evident in the schlieren photographs of figure 5. Inasmuch as no significant degradation in free-stream Mach number occurred over the entire survey length of 58 diameters, it is believed that the flow disturbances were small and did not significantly affect flow-field development.

Air-Air Velocity Data

$M_a = 1.268$.- An air-air mixing study of circular, coaxial, parallel compressible air jets has been reported in reference 6. The jets had total temperatures of approximately 300 K and exhausted to the atmosphere. Mixing of the jets was studied with the use of tracer gas. Figure 7(c) presents the center-line velocity data for a Mach 0.813 inner jet surrounded by a Mach 1.268 outer jet. Large initial boundary layers were prevalent in both jets and caused the initial decrease in center-line velocity shown in figure 7(c). Further details about these data and the air-air data in figure 7(d) may be found in reference 6.

$M_a = 1.302$.- Center-line velocity data from reference 6 for air-air mixing of a Mach 0.942 circular coaxial jet surrounded by a Mach 1.302 jet is given in figure 7(d). The test conditions differ from those for the air data in figure 7(c) only in the slightly larger values of M_a and M_j and the use of a larger center nozzle. Data obtained at $x/d = 49$ are reported to be of uncertain accuracy because the outer mixing boundaries had extended into the mixing zone; this necessitated large corrections to the data at this station.

Comparison of Unified and Z-Difference Viscosity Models

Theoretical center-line velocity distributions for hydrogen-air mixing and air-air mixing just discussed were generated by using the unified and Z-difference viscosity models and are presented in figure 7. Computations were started at the nozzle exit in two cases in order to support the contention that the unified model would lose its validity near the exit of an axisymmetric nozzle.

It is evident from inspection of figure 7(a) that the unified model drastically overpredicts the rate of decay of the center-line velocity for $M_a = 1.32$ when computations are started at the nozzle exit plane. Computations were also started at a downstream station ($x/d = 9.58$) with the initial conditions obtained from the actual measured profiles. Again, the unified model predicts much too rapid mixing when the recommended constant πk_2 of 0.018 was used. Calculations indicated that a constant πk_2 of 0.00306 was a more reasonable value for use with the unified model and the present data as shown by the dashed curve in figure 7(a).

The measured profiles at $x/d = 9.58$ were also used to initiate computations using the Z-difference model for the hydrogen-air data of figure 7(a) and a constant k value of 0.028. It is evident that the Z-difference model is superior to the unified model for these data.

Figure 7(b) presents the results of using the measured profiles at $x/d = 4.31$ to initiate calculations for the $M_a = 2.50$ data with both the unified and Z-difference models. Again the unified model with its recommended constant πk_2 of 0.018 greatly overpredicts the center-line velocity decay. Calculations indicated that a value of πk_2 of 0.00101 was more applicable to the data as evident in the right-hand curve of figure 7(b).

The center-line velocity decay predicted by using the Z-difference model and a constant k of 0.0255 is also shown in figure 7(b). As for the Mach 1.32 data of figure 7(a), the unified model prediction deviates more sharply from the data than the Z-difference model prediction. Neither model predicts the decay of center-line velocity below free-stream velocity as exhibited by the data. A discussion as to why the calculations do not predict the center-line velocities below free-stream velocity may be found in the section entitled "M_a = 2.50 Hydrogen-Air Radial Profiles."

The center-line velocity distribution predicted for the $M_a = 1.268$ air data by using the unified model with calculations initiated at the nozzle exit is shown in figure 7(c). As for the hydrogen-air data, the predicted center-line velocity change is much too rapid. Since the velocity trends appeared to be correct, the unified model solution was calculated for a constant πk_2 of 0.00356. Comparison of this solution with the Z-difference model solution (k = 0.0078) shown in figure 7(c) clearly shows the superiority of the Z-difference model.

Theoretical center-line velocity distributions for the $M_a = 1.302$ air data are presented in figure 7(d). Calculations were initiated at $x/d = 17.2$ and used the experimentally determined profiles from reference 6. The unified model together with the recommended value of πk_2 of 0.018 again overpredicts the mixing rate and associated velocity increase. (Similar calculations initiated at $x/d = 25$ are presented in fig. 12 of ref. 3. A similar trend of overpredicting the mixing rate was exhibited.) When the constant πk_2 was reduced to 0.0094, the unified model solution was only slightly less satisfactory than the Z-difference model solution with $k = 0.0098$, as evidenced by the curves in figure 7(d).

For all data considered, it is concluded that the Z-difference model correlates data more satisfactorily than the unified model. The recommended value of the empirical constant πk_2 of 0.018 for use with the unified model was unsatisfactory and too large by a factor of approximately 2 to 6. The unified model may find an application to the mixing of streams of nearly equal velocities across the mixing zone, where the mixing-zone width of the Z-difference model becomes indefinite, but where a mass flux difference exists between the streams. It is a desirable feature of any eddy viscosity model to be able to correlate data by initiating computations at the nozzle exit and to proceed downstream with the computations in a continuous manner. Satisfactory correlation and continuous computations from the nozzle exit were not possible with the unified model for the axisymmetric mixing data presented. Unsatisfactory correlation appears to result from an incorrect assumption that the viscosity is related to the mass flow defect or excess across the mixing zones. Continuous computations from the nozzle exit were not possible because of a poor approximation to the characteristic length of the near-field mixing zone.

Comparison of Z-Difference and Cohen Viscosity Models

In figure 8, center-line velocity data of figure 7 are compared with theoretical center-line velocity distributions computed by using the Z-difference and Cohen viscosity models. All Cohen model solutions presented employ values of the constants f^* and m_1 of 1.0 and 0.4, respectively, as recommended in reference 4.

The center-line velocity distribution corresponding to the $M_a = 1.32$ hydrogen-air data and the Z-difference model is presented in figure 8(a). The computed velocity distribution is seen to be low in the region of jet exit, high in the immediate far field, and to only approach the data at the most downstream stations.

The center-line velocity distribution computed by using the Cohen model and a value of k_3 of 0.002 is also presented in figure 8(a). (The values of turbulent Lewis number and turbulent Prandtl number quoted for the Cohen model calculations in figs. 8(a) and 8(b) are for later reference purposes.) Since the ratio of free-stream velocity to jet velocity was 0.366 (less than 0.4), equation (8) was used to initiate the Cohen model computations. As computations proceeded to an x/d of 6.81, the ratio of free-stream velocity to center-line velocity increased to 0.4; this necessitated a viscosity model change to equation (9), as recommended in reference 4. The Cohen model is seen to give a much better correlation of the center-line velocity than the Z-difference model for the data of figure 8(a).

In figure 8(b), the result of computations using the Z-difference model is shown for the $M_a = 2.50$ hydrogen-air data. The Z-difference model solution is seen to be low in correlating the velocity near the nozzle exit and high in the downstream region, as was the Z-difference solution shown in figure 8(a).

The Cohen model solution, as computed by use of equation (9) for $u_a/u_j > 0.4$, is also shown in figure 8(b) for a value of k_3 of 0.00129. The correlation with the $M_a = 2.50$ hydrogen-air data is seen to be good. The solution deviates from the data only when the center-line velocity data decreases to values below the free-stream velocity.

The Z-difference and Cohen model correlations for the air-air mixing data are shown in figures 8(c) and 8(d). The Cohen model solutions were computed by the use of equation (8) for $u_a/u_j > 0.4$. Both models correlate the air-air velocity data with approximately equal accuracy. Relative to each other, the Cohen model predicts slightly more rapid mixing in the near field and less rapid mixing in the far field than the Z-difference model.

It is concluded from the discussion of the correlations in figure 8 that the kinematic viscosity model of Cohen is superior to the Z-difference model. However, the Cohen model required empirical constants ranging from 0.00129 to 0.0038 compared with a recommended value from reference 4 of approximately 0.008. Since the empirical constants were significantly different from the recommended value, a calculation was performed for conditions corresponding to a known solution of Cohen in reference 5. The results obtained from using the present calculation technique and that given in reference 5 were found to be in good agreement, and the empirical constant was near 0.008. However, the parameter m_1 (see eq. (9)) was taken to be 0.6 for this calculation, which has a direct effect on the value of the required constant.

It was anticipated that the Z-difference model would correlate the hydrogen-air data in a more satisfactory manner than occurred, particularly since the model satisfactorily correlated the air-air data of reference 6. Inasmuch as the Cohen model was superior to the Z-difference model, a study was made to determine the significant differences in the two models. If one considers the Cohen model given by equation (9) and reduces it to primary variables, the result is the following expression:

$$\epsilon_t = \text{Constant}\left[\frac{\rho_o u_o + \rho_a u_a}{\left(\rho_a + \rho_o\right) u_o}\right] b u_o \qquad (12)$$

In equation (12), the empirical constant has been combined with other parameters which are only a function of test conditions. As pointed out by Cohen in reference 5, the term in the brackets is not a strong function. Upon comparison with equation (3), it is noted that the two models differ primarily in the definition of the mixing width and in the use of a kinematic viscosity in the Cohen formulation. Calculations were made with the two different mixing-width definitions. It was found that the mixing rate for a model was not significantly affected by changing mixing-width definitions, as long as the magnitude of the empirical constant was adjusted. It was concluded that the primary difference between the Cohen model of equation (9) and the Z-difference model was in the use of kinematic viscosity values in the Cohen model. Calculations were made to support this conclusion and the results are discussed in the next section.

Comparison of Kinematic Z-Difference and Cohen Viscosity Models

A kinematic form of the Z-difference model was developed and is given by

$$\epsilon_t = k_4 z u_o \qquad (13)$$

In equation (13) all parameters are as previously defined with the exception of a new empirical constant k_4.

Figure 9 compares the results of computations using the kinematic Z-difference model and the Cohen viscosity model with the four sets of data previously discussed. In figure 9(a), the velocity distribution from the kinematic Z-difference model is seen to give excellent correlation of all data downstream of the velocity core for the $M_a = 1.32$ hydrogen-air data. A value of k_4 of 0.0175 was used in the correlation. The Cohen model correlation is seen to better predict the velocity core length but was less satisfactory than the kinematic Z-difference model in predicting downstream velocities. Comparison of the Z-difference model solution of figure 8(a) and the kinematic Z-difference model solution of figure 9(a) indicates that substantial better correlation was achieved with the kinematic Z-difference model.

A comparison of the Cohen model solution of figure 8(a) for $N_{Pr} = 0.8$ and $N_{Le} = 1.0$ with the Cohen model solution of figure 9(a) for $N_{Pr} = 1.0$ and $N_{Le} = 1.0$ shows only a very slight effect on the value of N_{Pr}. This comparison supports the procedure of determining the empirical constant by correlating the velocity distribution and then determining the proper value of N_{Pr} and N_{Le} by correlating the concentration distribution.

In figure 9(b), the velocity distribution resulting from computations using the kinematic Z-difference model is seen to be slightly poorer than the Cohen viscosity model solution for the $M_a = 2.50$ hydrogen-air data. Differences in trends between the Cohen and kinematic Z-difference model solutions are due almost entirely to the bracketed term in equation (12). Comparison of the Z-difference model solution of figure 8(b) and the kinematic Z-difference model solution of figure 9(b) again indicates the superiority of the kinematic Z-difference model.

In figures 9(c) and 9(d), kinematic Z-difference model solutions and Cohen model solutions are presented for the air-air mixing data. For the air-air data, no significant difference between the kinematic Z-difference model solutions of figures 9(c) and 9(d) and the Z-difference model solutions of figures 8(c) and 8(d) is noted. The differences in the constants employed with the models (0.0078 as opposed to 0.0076 and 0.0098 as opposed to 0.0106) are considered beyond the accuracy of the data and correlation method.

On the basis of these comparisons, it is concluded that both the Cohen and the kinematic Z-difference eddy viscosity models permitted correlation of the velocity distributions satisfactorily and that a kinematic form of the eddy viscosity, which provides radial variations as well as axial variations in dynamic eddy viscosity through use of the local density, is superior to an eddy viscosity, which permits variations only in the axial direction. The latter conclusion is based upon the fact that an eddy viscosity which employed the local density permitted correlation of both air-air and hydrogen-air mixing data, whereas an eddy viscosity which employed the center-line density satisfactorily correlated air-air mixing data only. The conclusion is in agreement with the results of reference 15 which concluded that "the ultimate model for the turbulent transport coefficients must include variation in the axial as well as the radial direction." The requirement for a kinematic eddy viscosity formulation found herein is also in agreement with a conclusion of reference 16 which reported a study of turbulent boundary layers with mass addition, combustion, and pressure gradients. In reference 16, it was concluded that agreement between experimental and predicted velocity profiles validated the assumption that the

Reynolds stress (which is directly related to the eddy viscosity by the velocity gradient) is kinematic in nature.

Center-Line Mach Number and Hydrogen Mass Fraction Correlations

Since both the kinematic Z-difference and the Cohen eddy viscosity models were satisfactory in correlating the velocity distributions, both models were used to correlate the center-line Mach number and the center-line hydrogen mass fraction distributions. These correlations, in particular the mass fraction distributions, determine representative values of the turbulent Prandtl number and turbulent Lewis number. Concentration data corresponding to the air-air data need no further consideration inasmuch as the velocity correlations, and therefore the concentration distributions, are essentially identical to those of reference 6. In reference 6, the concentration correlation for the air-air data was found to be insensitive to the actual magnitudes of N_{Le} and N_{Pr} and depended solely upon the turbulent Schmidt number N_{Sc}. In reference 6 a turbulent Schmidt number of 0.6 was found to be representative of the $M_a = 1.268$ and $M_a = 1.302$ data.

The center-line Mach number distribution for $M_a = 1.32$ hydrogen-air mixing is presented in figure 10(a). The center-line hydrogen mass fraction distribution for the same condition is presented in figure 10(b). Center-line Mach number and mass fraction distributions computed by using the Cohen and the kinematic Z-difference models are also shown in figure 10. In figure 10(a), the center-line Mach number distribution is best correlated by the kinematic Z-difference model with $N_{Le} = 1.0$ and $N_{Pr} = 0.9$ $(N_{Sc} = 0.9)$. The Cohen model solutions are seen to exhibit trends which diverge significantly from the data at x/d greater than approximately 15. Note that the two solutions shown for the Cohen model in figure 10(a) are for different values of N_{Pr} (0.8 and 1.0) but for values of N_{Le} of unity. It is evident that the Cohen model solution with $N_{Le} = 1.0$ and $N_{Pr} = 1.0$ best approximates the Mach data.

In figure 10(b), the hydrogen mass fraction distribution is well correlated by the kinematic Z-difference model with $N_{Le} = 1.0$ and $N_{Pr} = 0.9$ for x/d greater than approximately 7. However, the Cohen model solution with $N_{Le} = 1.0$ and $N_{Pr} = 1.0$ is seen to better predict the concentration core length. On the basis of the correlations of figures 9(a), 10(a), and 10(b), it is apparent that the kinematic Z-difference model correlates a larger portion of the flow field than the Cohen model.

The center-line Mach number distribution for $M_a = 2.50$ hydrogen-air mixing is presented in figure 10(c). The center-line hydrogen mass fraction distribution for the same test condition is presented in figure 10(d). It is noted in figure 10(c) that the kinematic Z-difference model solution with $N_{Le} = 1.0$ and $N_{Pr} = 1.0$ appears to best correlate the data. However, the kinematic Z-difference model solution with $N_{Le} = 1.0$

and $N_{Pr} = 0.9$, as was used in the correlations of figures 10(a) and 10(b), is believed to be within the accuracy of the data and correlation technique. In figure 10(c) the Cohen model solution with $N_{Le} = 1.0$ and $N_{Pr} = 1.0$ exhibits the same trend as in figure 10(a), that is, diverging from the data in the region beyond $x/d = 15$.

In figure 10(d), the mass fraction distribution is best correlated by the Cohen model solution with $N_{Le} = 1.0$ and $N_{Pr} = 1.0$. It is indeterminate whether values of $N_{Le} = 1.0$, $N_{Pr} = 1.0$ or $N_{Le} = 1.0$, $N_{Pr} = 0.9$ are better for correlation using the kinematic Z-difference model mass fraction distributions of figure 10(d) because the $N_{Le} = 1.0$, $N_{Pr} = 1.0$ solution results in better correlation of the mass fraction data for x/d less than approximately 13 and the $N_{Le} = 1.0$, $N_{Pr} = 0.9$ solution results in better correlation for data farther downstream. As in reference 6, the concentration correlation was found to be insensitive to the actual magnitude of N_{Le} and N_{Pr} but depended only upon N_{Sc}. The sole dependence upon N_{Sc} is believed to be due to the fact that no significant transfer of heat is involved in the mixing process.

In reference 8, values of N_{Sc} ranging from 0.3 to 2.3 were reported for hydrogen-air, helium-air, and argon-air jets. (Some of the air jets considered in ref. 8 were heated.) No dependence of N_{Sc} upon molecular weight was observed. Derivatives were obtained from experimental data in the determination of N_{Sc} in reference 8; thus, some scatter was undoubtedly introduced during computations due to data uncertainties. Reference 17 reported a value of N_{Sc} near 0.7 for coaxial nearly equal density jets; this value closely agrees with results reported in reference 6. Reference 2 also reported a value of N_{Sc} near 0.7 for carbon-dioxide—air and hydrogen-air jets in the downstream region. The various calculation techniques used by different investigators in determining N_{Sc} make valid comparison difficult. As N_{Sc} is a measure of the ratio of concentration to velocity potential core length, it is difficult to conceive of N_{Sc} as being other than near unity for hydrogen-air mixing. This follows from the fact that the velocity is extremely sensitive to hydrogen concentration and, thus, when the local hydrogen concentration changes, it would be closely accompanied by a change in velocity.

$M_a = 1.32$ Hydrogen-Air Radial Profiles

Radial velocity profile data obtained from the $M_a = 1.32$ hydrogen-air test are presented in figures 11(a) and 11(b). Radial hydrogen mass fraction profile data from the $M_a = 1.32$ test are presented in figures 11(c) and 11(d). Correlations generated by using the Cohen viscosity model and the kinematic Z-difference model and the constants previously determined are also shown in the figures.

The velocity data presented in figures 11(a) and 11(b) are seen to be generally self-consistent with the exception of the profile at $x/d = 15.4$ where some unexplained asymmetry is noted. The velocity is seen to be nearly uniform at $x/d = 63.6$; however, the hydrogen mass fraction is approximately 1.6 percent on the center line indicating the total pressure distribution is not uniform. In figure 10(a) it is seen that the center-line Mach number at $x/d = 63.6$ is 1.18 as opposed to a free-stream Mach number of 1.32, which indicates mixing to a uniform condition has not been achieved.

The velocity profile used to initiate the mixing calculations at $x/d = 0.0$ is shown as a solid line in figure 11(a). Because the data for $x/d = 0.0$ were for a higher temperature (and thus a higher velocity) than the remainder of the data, a lower more representative velocity profile was used to initiate the calculations. Analytical solutions were not possible beyond approximately 32 jet diameters from the nozzle exit because the mixing width used in the viscosity models fails as the velocity becomes uniform. Therefore, no correlations are presented for $x/d = 42.8$ and 63.6. With the exception of $x/d = 5.51$, the kinematic Z-difference viscosity model (dashed lines in figs. 11(a) and 11(b)) is seen to give slightly better correlation than the Cohen viscosity model (solid lines in figs. 11(a) and 11(b)) for the $M_a = 1.32$ velocity data.

The hydrogen mass fraction profile data in figures 11(c) and 11(d) exhibit uniform trends and good repeatability throughout the range of the measurements. (Note the scale change between figs. 11(c) and 11(d).) The poorest data appear to exist near the profile maximum at $x/d = 9.58$ which is in the region of large axial gradients and large fluctuations immediately downstream of the potential core.

As was found with the velocity correlation, the kinematic Z-difference solution results in slightly better correlation than the Cohen solution for all stations other than $x/d = 5.51$.

$M_a = 2.50$ Hydrogen-Air Radial Profiles

Radial velocity profile data obtained from the $M_a = 2.50$ hydrogen-air test are presented in figures 12(a) and 12(b). Radial hydrogen mass fraction profile data are presented in figures 12(c) and 12(d). Correlations generated by using the kinematic Z-difference and Cohen viscosity models and the constants previously determined are also shown in the figures.

The velocity profile for $x/d = 0.0$ (fig. 12(a)) is noted to have a slightly larger boundary layer in the airstream than the $M_a = 1.32$ data (fig. 11(a)). In order to limit the number of input points to the computer program, and thus limit the computational time to a reasonable amount, the actual measured boundary layer was approximated by the solid line shown in figure 12(a). It was found during computations that a step velocity profile could be satisfactorily used as input as long as only center-line correlation was attempted. However, when considering correlation of radial profiles, the actual measured profile must be used as input. Some possible effect of the approximation of the initial profile may be seen in figure 12(a) for $x/d = 4.31$ and 8.75. However, the effect of the wake resulting from the finite nozzle lip thickness is impossible to separate completely from the initial boundary-layer approximation.

As was found during the center-line velocity correlation, the Cohen viscosity model solution is a better approximation of the $M_a = 2.50$ hydrogen-air data. However, neither model predicts the reduction in center-line velocity to below free-stream velocity shown in figure 12(b) for $x/d = 19.8$, 37.3, and 58.0. A study of the finite-difference technique employed in the analysis (ref. 11) indicates that once a uniform velocity profile is obtained, no further change in velocity is permitted. Furthermore, the viscosity models fail as the velocity profile approaches uniformity, due to employing a mixing width based on velocity. Thus, both the analysis employed and the eddy viscosity models prevent any computation of center-line velocity values below free-stream values.

The hydrogen mass fraction data in figures 12(c) and 12(d) exhibit wider spreading than the solutions predicted by either viscosity model, particularly for $x/d = 8.75$ and 15.4. It is interesting that these two axial stations were high in integrated-mass-flow ratio. The theoretical solutions of figures 12(c) and 12(d) indicate a possible bias in the data toward high values of concentration in this region of large radial gradients.

The Cohen viscosity model solution is seen to give better correlation than the kinematic Z-difference viscosity model solution for the $M_a = 2.50$ hydrogen-air data. Solutions were not possible for either viscosity model for $x/d = 37.3$ and 58.0 because the mixing width used in the models failed near $x/d = 30$ as the velocity profiles approached the uniform velocity condition.

The data and empirical constants employed herein are summarized in table II. Solutions beyond the region of application of the two viscosity models used herein can be generated by use of a constant viscosity, inasmuch as the regions are far downstream of the nozzle exit and should be approaching the boundary condition of uniform viscosity at infinity. Such computations were not made herein because they are in a region where application to scramjet combustor design would involve interaction between adjacent jets and, thus, involve an entirely different physical problem.

CONCLUDING REMARKS

An investigation of the compressible turbulent mixing of coaxial concentric hydrogen-air jets has been conducted. Hydrogen mass fraction profiles and velocity profiles were acquired for airstream Mach numbers of 1.32 and 2.50 corresponding to hydrogen jet Mach numbers of 0.89 and 0.91, respectively. These two sets of hydrogen-air data and two sets of air-air data (the air-air data from a previous study) have been satisfactorily correlated. For the data correlated, the ratio of jet velocity to free-stream velocity ranged from 0.648 to 2.730 and the ratio of jet mass flux to free-stream mass flux per unit area ranged from 0.647 to 0.0725. The total-temperature ratios of the streams for all data considered was near unity.

Three different eddy viscosity models were incorporated into a finite-difference-type analysis to test their validity in correlating the data. The kinematic eddy viscosity model of Cohen and a modified form of an eddy viscosity model used in a previous study both satisfactorily correlated the data.

A formulation of eddy viscosity which was previously employed to correlate air-air data and which only allowed axial variation in eddy viscosity was unsatisfactory in correlating the hydrogen-air data. It was found that a kinematic form of eddy viscosity which allowed radial variation as well as axial variation in dynamic eddy viscosity through incorporation of the local density was essential in order to correlate both the air-air and hydrogen-air data.

A formulation of eddy viscosity developed by Schetz, termed the "unified eddy viscosity model," which is based on a mass flow defect (or excess) across the mixing region, proved unsatisfactory in correlating the axisymmetric data considered herein.

Turbulent Schmidt numbers N_{Sc} used to correlate the hydrogen-air data were of the order of 0.9 to 1.0. The air-air data have been previously correlated with a value of N_{Sc} of 0.6.

Empirical constants used to correlate the data are, as yet, an unknown function of test conditions. The empirical constants used with the eddy viscosity models used herein varied by a factor of between 2 and 3 for the data considered. Correlation of a large quantity of data should permit a determination of the proper value of the constant to employ for given test conditions.

Langley Research Center,
National Aeronautics and Space Administration,
Hampton, Va., August 24, 1971.

APPENDIX A

VELOCITY AND HYDROGEN MASS FRACTION FOR $M_a = 1.32$ and $M_j = 0.89$[a]

x/d = 0.0[b]

y/d	M	u
-6.595	0.368	126
-6.565	.897	289
-6.538	1.055	331
-6.476	1.218	371
-6.437	1.284	386
-6.317	1.318	394
-6.203	1.324	395
-5.965	1.326	395
-5.612	1.324	395
-5.193	1.322	394
-4.729	1.322	394
-4.262	1.322	394
-3.790	1.317	394
-3.357	1.328	396
-2.881	1.326	395
-2.471	1.324	395
-2.029	1.320	394
-1.628	1.320	394
-1.244	1.309	392
-.975	1.294	388
-.843	1.271	383
-.776	1.245	377
-.697	1.204	368
-.649	1.153	355
-.591	1.079	337
-.565	1.023	323
-.543	.961	306
-.538	.823	268
-.490	.621	781
-.472	.735	911
-.459	.772	952
-.432	.817	1001
-.384	.852	1039
-.340	.862	1049
-.274	.872	1060
-.199	.878	1066
-.154	.882	1070
-.097	.884	1072
-.018	.886	1074
.119	.886	1074
.251	.876	1064
.322	.868	1056
.393	.846	1032
.463	.760	938
.485	.615	773

y/d	M	u
0.525	0.374	128
.534	.823	268
.543	.996	315
.565	1.046	329
.604	1.138	352
.631	1.182	362
.675	1.227	373
.724	1.251	379
.803	1.280	385
.949	1.297	389
1.050	1.303	390
1.174	1.308	391
1.381	1.315	393
1.654	1.320	394
2.025	1.322	394
2.462	1.326	395
2.956	1.328	396
3.428	1.328	396
3.829	1.326	395
4.301	1.324	395
4.835	1.324	395
5.157	1.324	395
5.629	1.326	395
6.079	1.327	396
6.481	1.305	391
6.525	1.196	366
6.587	.968	308
6.617	.520	176

x/d = 5.51

y/d	M	u
-5.973	1.330	397
-5.537	1.330	397
-5.316	1.328	396
-5.126	1.327	396
-4.897	1.327	396
-4.429	1.328	396
-3.970	1.337	398
-3.485	1.338	398
-3.141	1.338	398
-2.682	1.339	399
-2.237	1.335	398
-1.738	1.334	398
-1.354	1.334	398
-1.103	1.324	396
-1.010	1.297	392
-.904	1.262	389
-.851	1.220	394
-.825	1.187	404
-.768	1.104	396
-.724	1.035	398
-.684	.948	395
-.635	.864	400
-.560	.783	425
-.441	.755	514
-.366	.783	616
-.313	.810	709
-.247	.840	807
-.384	.779	594
-.331	.802	680
-.163	.860	927
-.110	.864	1012
.009	.860	1060
.044	.856	1056
.124	.840	975
.194	.802	858
.221	.793	807
.265	.779	743
.313	.774	676
.344	.774	632
.424	.815	543
.481	.927	528
.534	1.087	520
.587	1.184	485
.618	1.227	466
.688	1.303	431
.812	1.332	400
1.090	1.338	398
1.518	1.340	399
1.998	1.343	400
2.515	1.345	400
2.973	1.344	400
3.428	1.343	400

y/d	α
-1.200	0.000
-1.129	.000
-1.129	.000
-.887	.004
-.816	.014
-.710	.040
-.635	.079
-.547	.146
-.547	.143
-.454	.223
-.313	.455
-.141	.792
-.141	.773
.000	1.000
.000	1.000
.119	.873
.119	.873
.194	.731
.194	.692
.251	.585
.432	.218
.432	.224
.525	.109
.525	.109
.578	.063
.635	.033
.666	.019
.666	.019
.715	.008
.816	.001
.816	.001
.882	.000
.882	.000
.966	.000

x/d = 9.58

y/d	M	u
-3.587	1.304	394
-3.137	1.302	394
-2.709	1.301	393
-2.316	1.304	394
-1.813	1.310	396
-1.394	1.274	387
-1.332	1.339	402
-1.187	1.321	402
-1.125	1.297	401
-1.107	1.295	402
-1.024	1.247	401
-1.001	1.232	401
-.922	1.165	404
-.869	1.103	408
-.825	1.044	411
-.794	.991	408
-.701	.902	421
-.596	.831	436
-.503	.782	450
-.335	.758	535
-.203	.777	677
-.097	.809	726
.057	.822	739
.199	.796	674
.322	.782	590
.463	.822	509
.534	.891	488
.613	.997	475
.644	1.044	463
.701	1.131	449
.741	1.209	446
.807	1.272	430
.904	1.323	412
1.050	1.343	404
1.275	1.345	403
1.544	1.345	403
1.937	1.343	403
2.418	1.339	402

y/d	α
-1.584	0.000
-1.381	.000
-1.235	.001
-1.068	.006
-1.068	.006
-.926	.020
-.926	.019
-.807	.046
-.807	.045
-.706	.081
-.706	.082
-.596	.123
-.596	.120
-.476	.177
-.476	.182
-.335	.263
-.335	.261
-.176	.480
-.035	.504
-.035	.480
.097	.492
.097	.492
.229	.413
.229	.413
.393	.256
.534	.140
.534	.144
.613	.091
.693	.049
.693	.049
.746	.026
.754	.030
.754	.031
.843	.012
.843	.014
.926	.004
.926	.004
1.063	.000
1.063	.000
1.187	.000

[a]Total temperatures of the air and hydrogen jets for each x/d are given in table I(a).

[b]Velocities tabulated for x/d = 0.0 were computed for a hydrogen jet total temperature of 295 K, inasmuch as this value was more representative of the entire data rather than the actual measured value of 306 K.

x/d = 15.44

y/d	M	u	y/d	α
-4.253	1.331	398	-1.504	0.000
-4.068	1.330	397	-1.068	.012
-3.768	1.325	396	-1.068	.013
-3.335	1.325	396	-1.068	.012
-2.991	1.331	398	-.878	.031
-2.550	1.331	398	-.878	.031
-2.268	1.330	397	-.613	.084
-1.871	1.327	397	-.613	.084
-1.513	1.319	396	-.494	.114
-1.328	1.302	397	-.362	.154
-1.213	1.269	398	-.216	.204
-1.103	1.203	394	-.009	.235
-.997	1.130	393	.150	.225
-.887	1.053	394	.309	.181
-.807	.988	393	.543	.106
-.688	.918	409	.741	.056
-.543	.851	427	.988	.015
-.441	.826	447	.988	.015
-.322	.820	479	1.116	.005
-.150	.820	528	1.116	.005
.075	.830	551	1.209	.002
.256	.842	529	1.209	.002
.410	.893	499	1.407	.000
.525	.959	483		
.631	1.066	483		
.715	1.141	478		
.803	1.218	467		
.887	1.269	451		
1.019	1.311	424		
1.271	1.327	399		
1.509	1.330	397		
1.932	1.331	398		
2.400	1.331	398		
2.846	1.331	398		

x/d = 25.2

y/d	M	u	y/d	α
-4.570	1.313	389	-2.444	0.000
-4.068	1.322	391	-2.021	.000
-3.573	1.325	392	-1.593	.001
-3.176	1.326	392	-1.390	.005
-2.797	1.327	392	-1.390	.005
-2.303	1.327	392	-1.156	.011
-1.862	1.323	392	-.940	.026
-1.372	1.294	397	-.940	.026
-1.200	1.259	401	-.715	.045
-1.072	1.216	404	-.715	.045
-.957	1.172	411	-.512	.066
-.891	1.142	412	-.512	.066
-.785	1.082	410	-.234	.090
-.657	1.032	415	-.234	.089
-.547	.996	421	-.071	.102
-.371	.947	428	-.071	.100
-.097	.919	443	.141	.098
.137	.922	443	.141	.099
.278	.933	438	.371	.085
.446	.960	431	.371	.086
.600	1.005	422	.587	.062
.719	1.049	414	.587	.062
.821	1.126	421	.812	.038
.957	1.193	417	.812	.038
1.081	1.241	411	1.072	.017
1.209	1.281	404	1.072	.016
1.407	1.311	397	1.244	.007
1.619	1.324	395	1.526	.002
2.007	1.327	393	1.526	.002
2.528	1.328	393	1.932	.000
2.943	1.327	392	1.932	.000
3.335	1.325	392		
3.953	1.321	391		

x/d = 42.8

y/d	M	u	y/d	α
-7.350	0.728	240	-3.282	0.000
-7.266	.829	270	-3.282	.000
-6.432	.949	303	-2.876	.000
-6.088	1.038	327	-2.876	.000
-5.625	1.143	353	-2.413	.000
-5.409	1.176	362	-2.413	.000
-5.170	1.223	373	-2.021	.001
-4.853	1.265	383	-2.021	.001
-4.363	1.306	392	-1.584	.006
-3.860	1.324	396	-1.584	.005
-3.485	1.332	398	-1.116	.016
-3.181	1.334	398	-1.116	.015
-2.793	1.334	398	-.671	.030
-2.290	1.330	398	-.671	.029
-1.884	1.314	399	-.190	.041
-1.544	1.278	401	-.190	.041
-1.249	1.223	401	-.031	.041
-1.010	1.164	399	-.031	.041
-.754	1.114	401	.216	.040
-.326	1.073	412	.657	.028
-.040	1.068	416	1.125	.016
.212	1.087	418	1.535	.006
.428	1.108	415	1.557	.005
.710	1.181	421	1.968	.001
.838	1.217	423	1.968	.001
1.063	1.257	421	2.413	.000
1.288	1.293	416	2.413	.000
1.654	1.324	406	2.828	.000
2.082	1.332	400		
2.515	1.332	398		
3.031	1.330	397		
3.432	1.320	395		
3.957	1.299	390		
4.443	1.259	381		
4.879	1.210	370		

x/d = 63.6

y/d	M	u	y/d	α
-8.091	0.633	212	-4.244	0.000
-7.650	.698	232	-3.763	.000
-7.187	.769	253	-3.763	.000
-6.776	.827	270	-3.388	.000
-6.304	.898	290	-2.925	.001
-5.872	.967	309	-2.501	.002
-5.457	1.037	327	-2.043	.004
-5.065	1.096	342	-1.566	.007
-4.690	1.145	354	-1.116	.010
-4.293	1.193	366	-.675	.014
-3.851	1.250	380	-.675	.015
-3.582	1.270	384	-.238	.017
-3.221	1.285	388	-.238	.017
-2.929	1.291	391	.172	.017
-2.607	1.296	393	.618	.015
-2.188	1.291	396	1.046	.011
-1.760	1.281	400	1.500	.008
-1.434	1.259	400	1.954	.004
-1.129	1.237	401	2.404	.002
-.874	1.214	400	2.837	.001
-.631	1.199	401	3.265	.000
-.371	1.188	402	3.710	.000
-.106	1.181	402	4.165	.000
.154	1.186	402	4.597	.000
.379	1.186	400		
.622	1.199	401		
.878	1.219	402		
1.121	1.241	403		
1.354	1.257	402		
1.654	1.274	400		
1.915	1.285	398		
2.294	1.291	395		
2.612	1.287	391		
3.018	1.274	387		
3.463	1.255	381		
3.900	1.224	374		
4.363	1.179	363		
4.672	1.133	351		
5.166	1.070	336		
5.598	.998	317		
6.075	.923	297		
6.604	.843	274		
7.147	.764	251		
7.747	.658	219		
8.365	.587	197		

APPENDIX B

VELOCITY AND HYDROGEN MASS FRACTION FOR $M_a = 2.50$ AND $M_j = 0.91$[a]

x/d = 0.0

y/d	M	u
-6.666	0.432	153
-6.591	.932	311
-6.512	1.548	461
-6.437	2.105	555
-6.159	2.499	603
-6.026	2.502	603
-5.572	2.494	603
-5.325	2.531	606
-4.862	2.538	607
-4.412	2.531	606
-3.922	2.538	607
-3.468	2.565	610
-3.168	2.586	612
-2.943	2.511	604
-2.493	2.520	605
-2.215	2.545	608
-1.990	2.524	606
-1.562	2.503	603
-1.394	2.461	599
-1.284	2.423	595
-1.134	2.363	588
-.904	2.240	573
-.746	2.067	549
-.578	1.732	496
-.547	1.600	471
-.499	.718	248
-.485	.309	403
-.468	.507	651
-.454	.644	815
-.446	.662	836
-.432	.718	901
-.415	.783	973
-.397	.819	1013
-.379	.857	1054
-.344	.877	1075
-.300	.896	1095
-.053	.907	1107
.154	.907	1107
.251	.907	1107
.353	.871	1068
.366	.865	1062
.384	.845	1040
.406	.815	1008
.424	.769	957
.446	.668	843

y/d	M	u
0.459	0.598	761
.472	.432	558
.485	.309	403
.503	1.098	357
.516	1.278	401
.543	1.522	455
.569	1.673	485
.596	1.760	500
.622	1.834	513
.688	1.975	536
.768	2.092	553
.860	2.204	568
.962	2.287	579
1.054	2.333	584
1.147	2.379	590
1.253	2.434	596
1.368	2.472	600
1.522	2.507	604
1.703	2.527	606
1.932	2.531	606
2.126	2.519	605
2.303	2.496	603
2.625	2.481	601
2.912	2.472	600
3.238	2.575	611
3.684	2.541	607
4.147	2.506	604
4.663	2.514	605
5.237	2.493	602

x/d = 4.31

y/d	M	u
-2.868	2.588	604
-2.673	2.567	602
-2.550	2.528	598
-2.334	2.503	596
-2.201	2.536	599
-2.012	2.593	605
-1.831	2.598	605
-1.610	2.577	603
-1.518	2.562	602
-1.407	2.531	599
-1.310	2.489	594
-1.218	2.414	586
-1.147	2.307	574
-1.072	2.214	562
-.949	2.135	552
-.874	2.066	543
-.785	1.967	540
-.701	1.835	569
-.649	1.675	625
-.596	1.424	656
-.560	1.206	642
-.521	1.025	639
-.476	.922	671
-.397	.874	778
-.326	.889	921
-.229	.897	1051
-.053	.897	1092
.106	.897	1092
.212	.897	1092
.375	.866	797
.468	.911	676
.521	1.040	656
.534	1.081	651
.551	1.182	658
.574	1.280	657
.626	1.534	628
.657	1.715	609
.693	1.805	577
.719	1.871	560
.776	1.947	542
.851	2.040	542
.931	2.097	546
1.001	2.160	555
1.076	2.202	560
1.178	2.303	573
1.266	2.446	590
1.407	2.542	600
1.548	2.579	604
1.840	2.588	604
2.109	2.562	602
2.409	2.484	594
3.044	2.547	600
3.335	2.525	598
3.706	2.557	601
4.010	2.557	601

y/d	α
-0.979	0.000
-.860	.001
-.768	.005
-.706	.019
-.662	.046
-.587	.114
-.587	.115
-.529	.197
-.529	.194
-.472	.316
-.472	.316
-.375	.549
-.300	.773
-.194	.959
-.079	1.000
.066	1.000
.066	1.000
.150	.945
.234	.841
.313	.692
.424	.402
.503	.255
.551	.168
.591	.115
.649	.053
.693	.026
.715	.017
.759	.007
.860	.001
.860	.001
.944	.000

x/d = 8.75

y/d	M	u
-4.173	2.529	590
-3.865	2.560	594
-3.591	2.555	593
-3.018	2.545	592
-2.722	2.545	592
-2.594	2.616	599
-2.400	2.591	597
-2.113	2.555	593
-1.641	2.518	589
-1.456	2.487	586
-1.328	2.407	577
-1.156	2.329	569
-1.041	2.237	560
-.909	2.148	561
-.856	2.066	558
-.807	1.988	559
-.750	1.800	573
-.706	1.639	590
-.688	1.503	576
-.600	1.179	584
-.534	1.023	595
-.300	.918	776
-.154	.918	906
-.026	.918	922
.194	.918	840
.340	.927	750
.507	1.037	650
.591	1.248	626
.657	1.485	609
.768	1.865	560
.851	2.104	565
.966	2.226	562
1.094	2.329	569
1.222	2.396	576
1.451	2.498	587
1.628	2.560	594
1.893	2.570	595
2.360	2.591	597
2.696	2.560	594
3.123	2.550	593

y/d	α
-1.076	0.000
-.776	.015
-.679	.058
-.543	.160
-.543	.165
-.419	.298
-.419	.300
-.247	.500
-.101	.651
.079	.591
.296	.441
.476	.256
.728	.035
.869	.006
.979	.001
1.103	.000

x/d = 15.36

y/d	M	u
-4.279	2.515	592
-3.600	2.531	593
-2.982	2.515	592
-2.607	2.510	591
-2.312	2.503	590
-1.901	2.489	589
-1.575	2.441	584
-1.376	2.386	583
-1.257	2.336	585
-1.107	2.255	586
-1.050	2.190	582
-.957	2.097	582
-.847	1.912	581
-.803	1.783	574
-.706	1.595	597
-.649	1.377	576
-.521	1.206	603
-.406	1.067	612
-.159	.995	658
.013	1.001	656
.176	1.051	658
.388	1.170	641
.503	1.295	621
.600	1.480	604
.693	1.699	586
.781	1.905	578
.856	2.027	567
.949	2.147	566
1.081	2.261	567
1.315	2.381	577
1.518	2.457	586
1.760	2.492	589
2.025	2.507	591
2.541	2.513	591
3.062	2.531	593
3.490	2.531	593

y/d	α
-1.429	0.000
-1.204	.004
-1.204	.004
-.984	.009
-.768	.028
-.657	.063
-.657	.064
-.525	.103
-.331	.198
-.106	.252
.110	.240
.331	.196
.556	.106
.657	.058
.759	.034
.882	.011
1.010	.004
1.107	.001
1.209	.000

[a]Total temperatures of the air and hydrogen jets for each x/d are given in table I(b).

x/d = 19.80

y/d	M	u
-5.290	2.494	588
-5.043	2.530	592
-4.831	2.488	588
-4.619	2.478	587
-4.394	2.473	586
-4.195	2.483	587
-3.940	2.509	590
-3.728	2.509	590
-3.476	2.499	589
-3.172	2.509	590
-2.793	2.514	591
-2.448	2.499	589
-2.126	2.488	588
-1.893	2.478	587
-1.650	2.440	583
-1.504	2.391	577
-1.341	2.324	570
-1.240	2.266	564
-1.107	2.171	556
-.993	2.052	548
-.878	1.870	536
-.821	1.775	532
-.763	1.610	517
-.657	1.411	517
-.591	1.303	516
-.490	1.191	522
-.349	1.083	528
-.088	1.034	537
.124	1.053	534
.326	1.138	544
.397	1.186	548
.472	1.247	550
.512	1.320	562
.565	1.398	565
.622	1.489	562
.701	1.659	569
.785	1.827	574
.874	1.993	576
.988	2.147	572
1.116	2.249	568
1.271	2.324	571
1.438	2.391	577
1.663	2.456	584
1.959	2.488	588
2.387	2.499	589
2.766	2.504	589
3.238	2.509	590
3.737	2.494	588

y/d	α
-1.332	0.000
-1.112	.002
-1.112	.002
-.891	.011
-.891	.012
-.785	.022
-.785	.023
-.679	.042
-.679	.042
-.560	.068
-.560	.068
-.560	.068
-.393	.102
-.393	.104
-.247	.122
-.247	.122
-.115	.123
-.115	.125
.009	.119
.009	.120
.168	.111
.304	.098
.428	.082
.565	.054
.710	.028
.869	.013
.984	.005
1.090	.002
1.196	.001
1.310	.000
1.310	.000

x/d = 37.3

y/d	M	u
-5.819	2.236	564
-5.581	2.385	582
-5.400	2.455	590
-5.140	2.503	595
-4.606	2.501	594
-4.235	2.501	594
-3.781	2.498	594
-3.282	2.488	593
-2.912	2.488	593
-2.448	2.498	594
-2.025	2.482	592
-1.721	2.434	587
-1.465	2.357	580
-1.328	2.300	576
-1.169	2.219	571
-1.068	2.121	568
-.971	2.052	570
-.856	1.918	565
-.772	1.812	560
-.693	1.722	556
-.626	1.618	545
-.534	1.524	543
-.428	1.442	540
-.216	1.356	540
.093	1.340	538
.243	1.372	536
.424	1.461	535
.604	1.626	551
.724	1.760	559
.843	1.946	571
.966	2.109	578
1.129	2.236	579
1.262	2.340	585
1.385	2.390	586
1.566	2.466	591
1.875	2.519	596
2.369	2.522	597
2.850	2.498	594
3.318	2.506	595
3.732	2.516	596
4.195	2.507	595
4.593	2.503	595
5.215	2.488	593

y/d	α
-2.056	0.000
-1.610	.000
-1.394	.001
-1.138	.003
-.953	.011
-.746	.019
-.746	.018
-.512	.038
-.203	.055
-.044	.059
.154	.055
.366	.045
.596	.031
.812	.017
1.024	.007
1.249	.002
1.451	.001
1.451	.001

x/d = 58.0

y/d	M	u
-4.407	2.459	588
-4.187	2.470	590
-3.931	2.470	590
-3.754	2.470	590
-3.529	2.470	590
-3.229	2.470	590
-2.978	2.470	590
-2.771	2.470	590
-2.307	2.462	589
-2.025	2.438	586
-1.804	2.405	583
-1.632	2.361	581
-1.557	2.338	580
-1.434	2.304	578
-1.306	2.234	574
-1.169	2.155	571
-1.063	2.099	571
-.975	2.036	568
-.856	1.962	566
-.785	1.900	562
-.666	1.799	555
-.551	1.717	549
-.335	1.604	544
-.110	1.562	547
.115	1.579	551
.251	1.604	551
.459	1.717	559
.569	1.815	568
.701	1.900	570
.847	2.023	576
.979	2.137	581
1.121	2.210	580
1.200	2.257	582
1.381	2.338	585
1.566	2.388	586
1.707	2.422	587
1.893	2.449	588
2.113	2.459	588
2.396	2.465	589
2.872	2.470	590
3.326	2.476	590
3.834	2.478	590
4.420	2.470	590
4.923	2.443	587
5.184	2.394	581

y/d	α
-2.201	0.000
-1.778	.000
-1.337	.003
-1.116	.006
-.891	.012
-.679	.018
-.450	.025
-.238	.032
-.132	.034
-.004	.035
.097	.035
.216	.033
.309	.031
.432	.026
.666	.019
.856	.013
.856	.013
1.081	.007
1.310	.003
1.769	.000
2.210	.000

APPENDIX C

DATA REDUCTION DETAILS

Primary variables measured in the test program included pitot pressures, total temperatures of both the hydrogen and the air jets, volumetric concentration of hydrogen, barometric pressure, and probe location. The hydrogen flow to the center nozzle was also determined by use of a calibrated sharp-edge orifice meter and redundantly measured by a variable-area orifice meter. (The flow rates determined by the two techniques were in agreement within 1 percent.)

The center of the flow field was assumed to coincide with the center of the hydrogen concentration (volumetric) profile. Since concentration and pitot measurements were not necessarily made at the same radial location, concentration values needed to determine velocity from the pitot-pressure measurements were taken from a plot of concentration as a function of probe location. The volumetric concentration values were reduced to hydrogen mass fraction values by assuming that the flow field consisted of a binary mixture of air and hydrogen. The mass fraction of hydrogen α is related, through the molecular weights, to the hydrogen volumetric concentration β by the following equation:

$$\alpha = \frac{2.016\beta}{2.016\beta + 28.96(1 - \beta)} \tag{C1}$$

The local molecular weight $\mathcal{M}$ is given by

$$\mathcal{M} = 2.016\beta + 28.96(1 - \beta) \tag{C2}$$

and the local gas constant by

$$R = \frac{\overline{R}}{\mathcal{M}} \tag{C3}$$

In equation (C3), $\overline{R}$ is the universal gas constant. (Note specific values are not assigned to parameters in this appendix if the values of the parameters vary with different systems of units. Any consistent system of units may be used in the evaluation of the equations presented.) The mixture specific heat C_p is expressed as

$$C_p = C_{p,h}\alpha + C_{p,a}(1 - \alpha) \tag{C4}$$

In equation (C4), $C_{p,h}$ is the specific heat at constant pressure of hydrogen and $C_{p,a}$ is the specific heat at constant pressure of air. The local total temperature T_t was computed by an energy balance as given by

$$T_t = \frac{\left[C_{p,h}\alpha T_{t,j} + C_{p,a}(1 - \alpha)T_{t,a}\right]}{C_p} \tag{C5}$$

In equation (C5), $T_{t,j}$ and $T_{t,a}$ are the measured total temperatures of the hydrogen and airstreams, respectively.

The local Mach number was computed from the Rayleigh pitot formula (see eq. (100) of ref. 18) for supersonic Mach numbers and from basic isentropic flow relations (see eq. (44) of ref. 18) for subsonic Mach numbers. A constant value of the specific-heat ratio γ of 1.4 was used in all data reduction. The static pressure was assumed uniform and equal to local atmospheric pressure throughout the flow field. Local static temperature was computed from the local total temperature (eq. (C5)), and the local Mach number was computed from isentropic flow relationships (see eq. (43) of ref. 18).

The local velocity is then computed from

$$u = M\sqrt{\gamma RT} \tag{C6}$$

In equation (C6), M is the local Mach number and T is the local static temperature.

Equation (1)

$$m_x = \sqrt{\gamma}\int_A \frac{\alpha p M}{\sqrt{RT}}\,dA$$

may also be evaluated to determine the total hydrogen flow rate m_x at any survey station. In this equation p is the static pressure, and the integral is evaluated over the area A for which α is greater than zero. The other parameters are as previously defined.

REFERENCES

1. Ferri, Antonio; Libby, Paul A.; and Zakkay, Victor: Theoretical and Experimental Investigation of Supersonic Combustion. ARL 62-467, U.S. Air Force, Sept. 1962.
2. Alpinieri, Louis J.: An Experimental Investigation of the Turbulent Mixing on Non-Homogeneous Coaxial Jets. PIBAL Rep. No. 789 (Contract No. AF 49(638)-217), Polytech. Inst., Brooklyn, Aug. 1963.
3. Schetz, Joseph A.: Unified Analysis of Turbulent Jet Mixing. NASA CR-1382, 1969.
4. Cohen, L. S.: A New Kinematic Eddy Viscosity Model. Rep. G211709-1, United Aircraft Corp., Jan. 1968.
5. Cohen, Leonard S.; and Guile, Roy N.: Investigation of the Mixing and Combustion of Turbulent, Compressible Free Jets. NASA CR-1473, 1969.
6. Eggers, James M.; and Torrence, Marvin G.: An Experimental Investigation of the Mixing of Compressible-Air Jets in a Coaxial Configuration. NASA TN D-5315, 1969.
7. Hopf, H.; and Fortune, O.: Diffusion Controlled Combustion for Scramjet Application. Part II – Programmer's Manual. Tech. Rep. 569 (Contract No. NAS1-5117), Gen. Appl. Sci. Lab., Inc., Dec. 1965.
8. Zakkay, Victor; Krause, Egon; and Woo, Stephen D. L.: Turbulent Transport Properties for Axisymmetric Heterogeneous Mixing. ARL 64-103, U.S. Air Force, June 1964. (Available from DDC as AD 604 008.)
9. Chriss, D. E.: Experimental Study of the Turbulent Mixing of Subsonic Axisymmetric Gas Streams. AEDC-TR-68-133, U.S. Air Force, Aug. 1968. (Available from DDC as AD 672 975.)
10. Henry, John R.: Recent Research on Fuel Injection and Mixing and Piloted-Ignition for Scramjet Combustors. Combustion Inst., 1969, pp. 1175-1182.
11. Edelman, R.: Diffusion Controlled Combustion for Scramjet Application. Part I – Analysis & Results of Calculations. Tech. Rep. 569 (Contract No. NAS1-5117), Gen. Appl. Sci. Lab., Inc., Dec. 1965.
12. Jeffery, P. G.; and Kipping, P. J.: Gas Analysis by Gas Chromatography. Macmillan Co., 1964.
13. Rogers, R. Clayton: A Study of the Mixing of Hydrogen Injected Normal to a Supersonic Airstream. NASA TN D-6114, 1971.
14. Reis, Victor H.; and Fenn, John B.: Separation of Gas Mixtures in Supersonic Jets. J. Chem. Phys., vol. 39, no. 12, Dec. 15, 1963, pp. 3240-3250.

15. Zelazny, S. W.; Morgenthaler, J. H.; and Slack, M. W.: Spatial Dependence of Turbulent Transport Coefficients in Dissimilar Coaxial Flows. Rep. No. 9500-920123, Bell Aerosystems Co., Mar. 1969.

16. Jones, J. W.; and Isaacson, L. K.: A Turbulent Boundary Layer With Mass Addition, Combustion, and Pressure Gradients. AFOSR 70-1428TR, U.S. Air Force, May 1970. (Available from DDC as AD 710 308.)

17. Forstall, Walton, Jr.; and Shapiro, Ascher H.: Momentum and Mass Transfer in Coaxial Gas Jets. J. Appl. Mech., vol. 17, no. 4, Dec. 1950, pp. 399-408.

18. Anon.: Equations, Tables, and Charts for Compressible Flow. NACA Rep. 1135, 1953.

TABLE I.- DATA SUMMARY

x/d	$T_{t,j}$	$T_{t,a}$	I
(a) $M_a = 1.32$; $M_j = 0.89$			
0.0	306	298	0.97
5.51	302	298	.84
9.58	293	303	.94
15.44	299	299	1.00
25.2	288	293	.98
42.8	291	299	1.00
63.6	293	299	1.04
(b) $M_a = 2.50$; $M_j = 0.91$			
0.0	300	324	0.9
4.31	298	316	1.27
8.75	302	308	1.25
15.36	294	310	1.29
19.8	301	309	.91
37.3	302	315	.88
58.0	302	313	.96

TABLE II.- CORRELATION SUMMARY

Data source	Gases	M_a	M_j	d, cm	u_j/u_a	$\rho_j u_j/\rho_a u_a$	$T_{t,j}/T_{t,a}$	Cohen viscosity model				Kinematic Z-difference model			
								k_3	N_{Le}	N_{Pr}	N_{Sc}	k_4	N_{Le}	N_{Pr}	N_{Sc}
Reference 6	Air-air	1.268	0.813	1.036	0.648	0.556	1.0	0.00252	1.0	0.6	0.6	0.0076	1.0	0.6	0.6
Reference 6	Air-air	1.302	.942	2.443	.736	.647	1.0	.0038	1.0	.6	.6	.0106	1.0	.6	.6
Present report	Hydrogen-air	1.32	.89	1.160	2.730	.171	1.0	.002	1.0	1.0	1.0	.0175	1.0	.9	.9
Present report	Hydrogen-air	2.50	.91	1.160	1.823	.0725	1.0	.00129	1.0	1.0	1.0	.0164	1.0	0.9 to 1.0	0.9 to 1.0

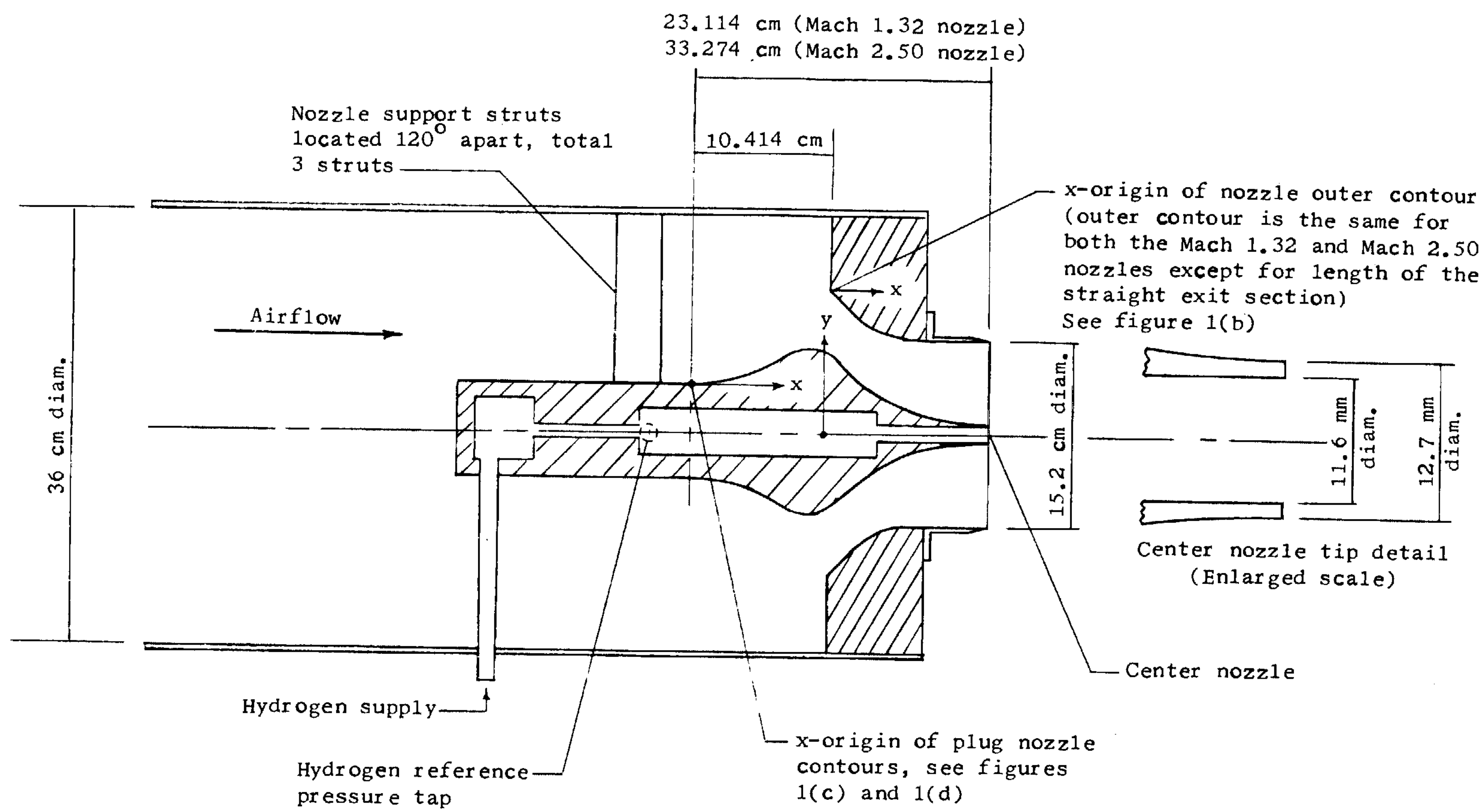

(a) General nozzle arrangement.

Figure 1.- Nozzle configuration.

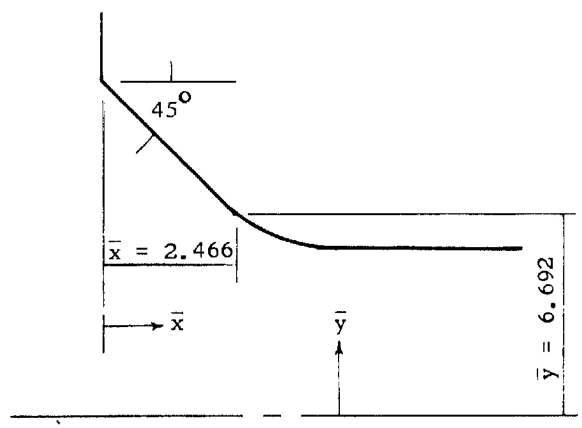

Contour coordinates	
$\bar{x}$	$\bar{y}$
2.466	6.692
2.580	6.600
2.780	6.446
2.980	6.326
3.180	6.236
3.380	6.170
3.580	6.124
3.780	6.076
3.980	6.044
4.180	6.028
4.380	6.014
4.580	6.000
4.780	6.000
6.000	6.000
10.000	6.000

Note: For location of the origin of the coordinates relative to the overall nozzle arrangement, see figure 1(a)

(b) Nozzle outer contour details.

Contour coordinates			
$\bar{x}$	$\bar{y}$	$\bar{x}$	$\bar{y}$
0.000	3.000	11.200	1.992
5.000	2.980	11.400	1.908
5.200	2.976	11.600	1.830
5.400	2.972	11.800	1.752
5.600	2.964	12.000	1.684
5.800	2.954	12.200	1.610
6.000	2.944	12.400	1.542
6.200	2.938	12.600	1.472
6.400	2.928	12.800	1.404
6.600	2.916	13.000	1.338
6.800	2.906	13.200	1.268
7.000	2.892	13.400	1.206
7.200	2.878	13.600	1.140
7.400	2.868	13.800	1.080
7.600	2.848	14.000	1.022
7.800	2.830	14.200	0.970
8.000	2.810	14.400	0.918
8.200	2.788	14.600	0.866
8.400	2.758	14.800	0.818
8.600	2.722	15.000	0.780
8.800	2.702	15.200	0.734
9.000	2.668	15.400	0.696
9.200	2.630	15.600	0.658
9.400	2.588	15.800	0.624
9.600	2.542	16.000	0.596
9.800	2.490	16.200	0.572
10.000	2.438	16.400	0.550
10.200	2.376	16.600	0.534
10.400	2.308	16.800	0.520
10.600	2.230	17.000	0.506
10.800	2.154	17.200	0.500
11.000	2.064	17.400	0.500
		18.200	0.500

(c) Mach 1.32 plug nozzle contour details.

Figure 1.- Continued.

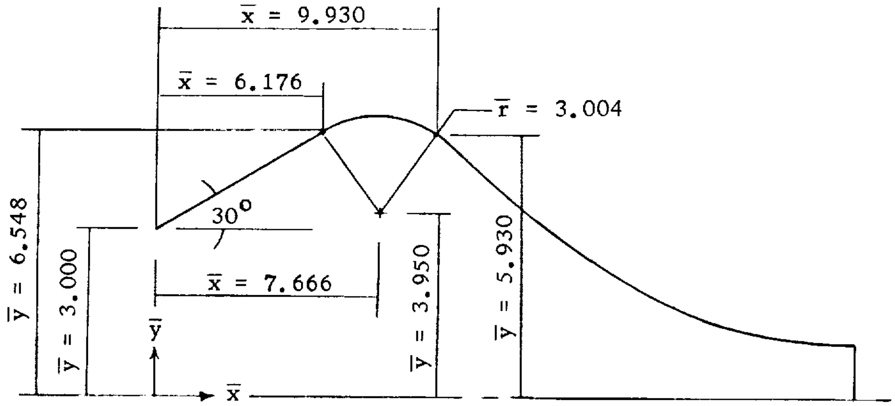

Contour coordinates					
$\bar{x}$	$\bar{y}$	$\bar{x}$	$\bar{y}$	$\bar{x}$	$\bar{y}$
9.930	5.930	15.200	2.522	20.600	1.022
10.000	5.854	15.400	2.446	20.800	0.984
10.200	5.632	15.600	2.370	21.000	0.950
10.400	5.424	15.800	2.294	21.200	0.914
10.600	5.216	16.000	2.224	21.400	0.880
10.800	5.030	16.200	2.158	21.600	0.846
11.000	4.850	16.400	2.096	21.800	0.810
11.200	4.690	16.600	2.030	22.000	0.776
11.400	4.520	16.800	1.960	22.200	0.748
11.600	4.378	17.000	1.912	22.400	0.720
11.800	4.234	17.200	1.854	22.600	0.692
12.000	4.102	17.400	1.788	22.800	0.672
12.200	3.970	17.600	1.732	23.000	0.644
12.400	3.842	17.800	1.680	23.200	0.620
12.600	3.720	18.000	1.624	23.400	0.602
12.800	3.610	18.200	1.572	23.600	0.586
13.000	3.498	18.400	1.510	23.800	0.572
13.200	3.394	18.600	1.468	24.000	0.554
13.400	3.290	18.800	1.406	24.200	0.540
13.600	3.200	19.000	1.364	24.400	0.536
13.800	3.100	19.200	1.316	24.600	0.526
14.000	3.014	19.400	1.274	24.800	0.520
14.200	2.928	19.600	1.230	25.000	0.512
14.400	2.840	19.800	1.192	25.200	0.506
14.600	2.758	20.000	1.144	25.400	0.502
14.800	2.682	20.200	1.098	25.600	0.500
15.000	2.598	20.400	1.060	25.800	0.500
				26.200	0.500

Note: For location of origin of coordinates relative to the overall nozzle arrangement, see figure 1(a)

(d) Mach 2.50 plug nozzle contour details.

Figure 1.- Concluded.

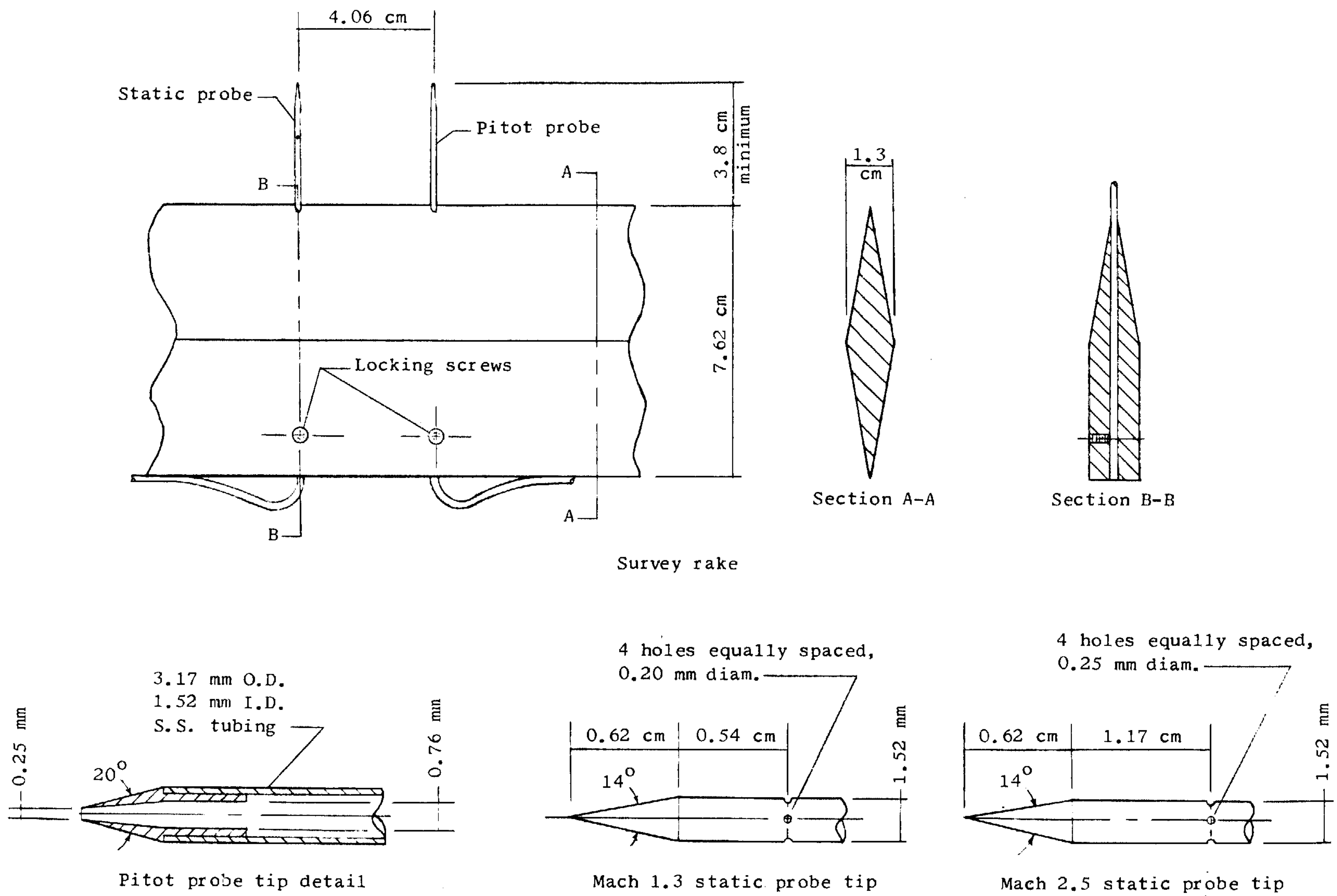

Figure 2.- Survey rake and probe details.

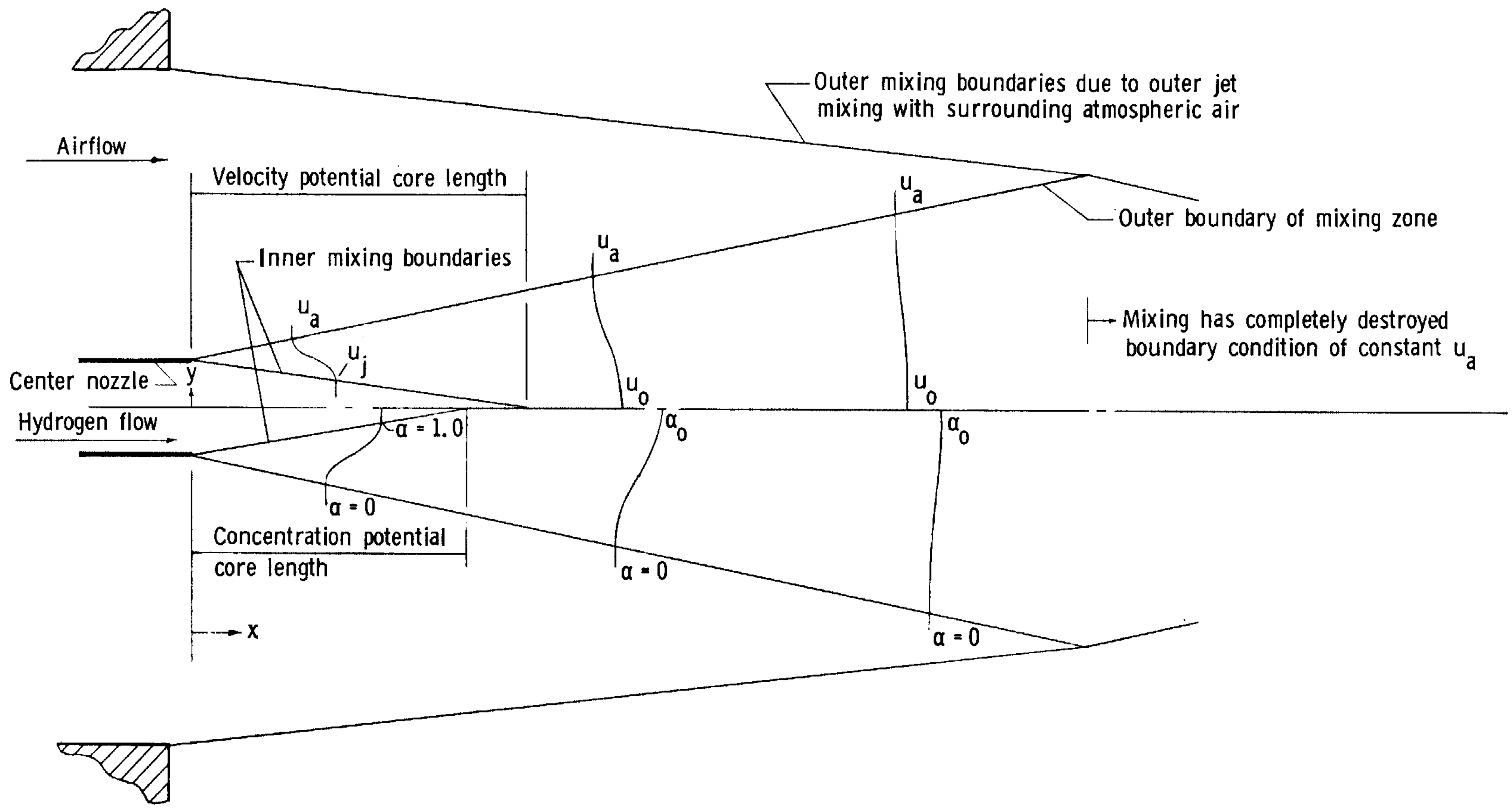

Figure 3.- Flow-field schematic.

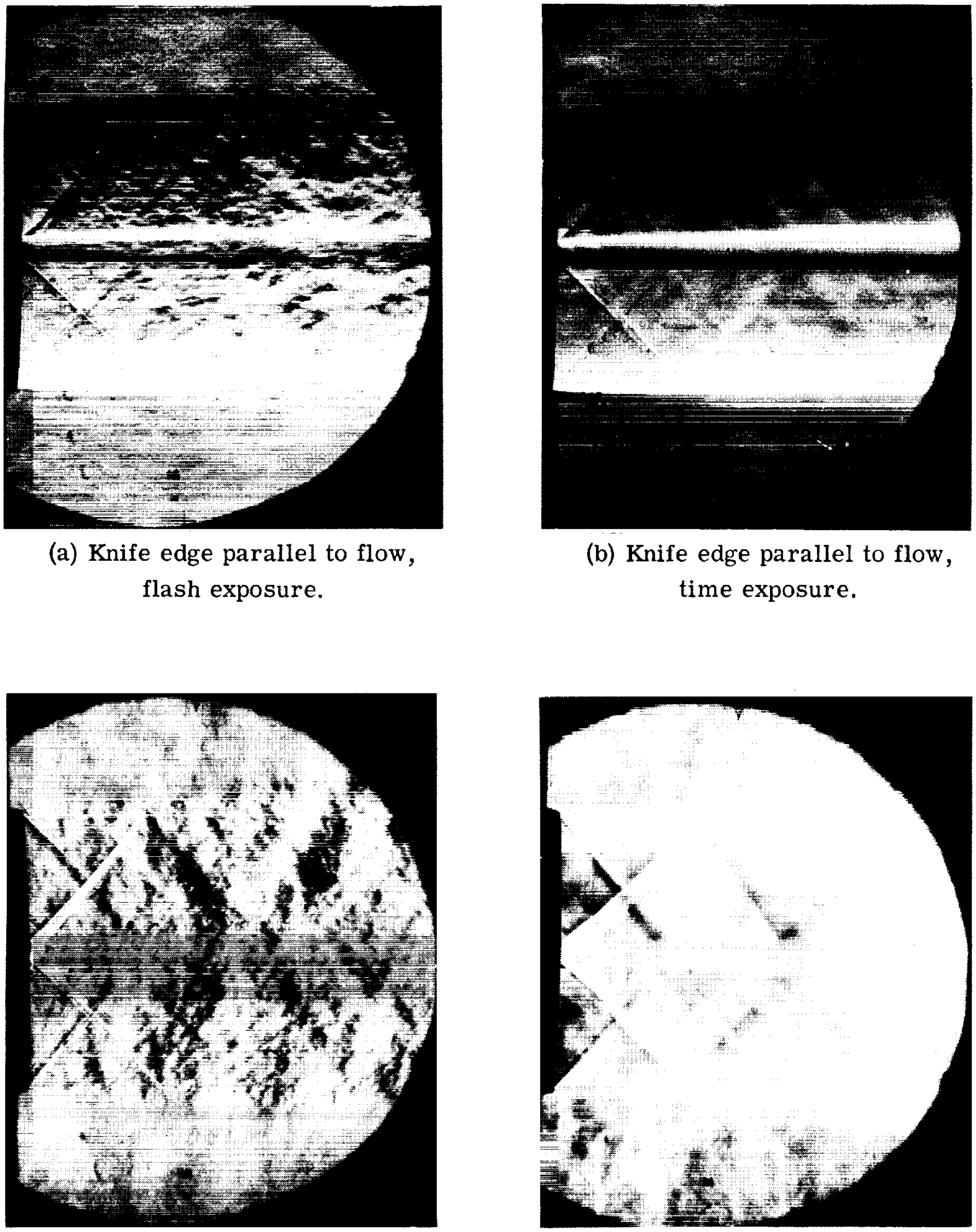

(a) Knife edge parallel to flow, flash exposure.

(b) Knife edge parallel to flow, time exposure.

(c) Knife edge normal to flow, flash exposure.

(d) Knife edge normal to flow, time exposure.

L-71-690

Figure 4.- Schlieren photographs for $M_a = 1.32$ and $M_j = 0.89$.

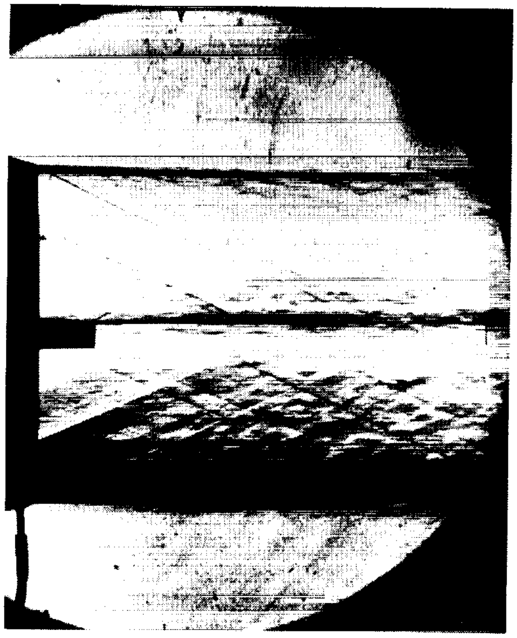

(a) Knife edge parallel to flow, flash exposure.

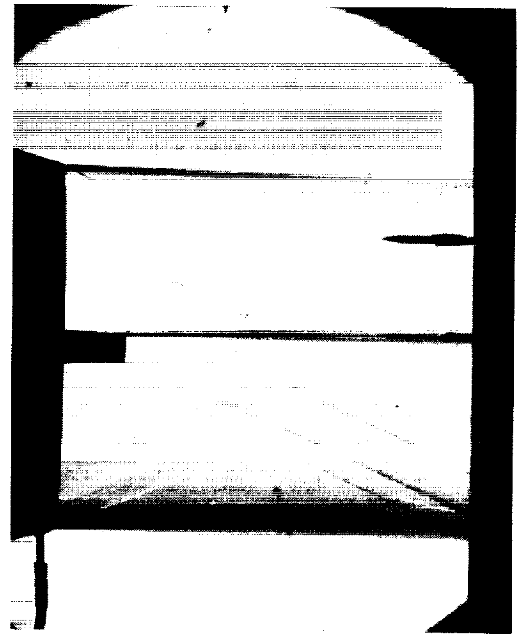

(b) Knife edge parallel to flow, time exposure.

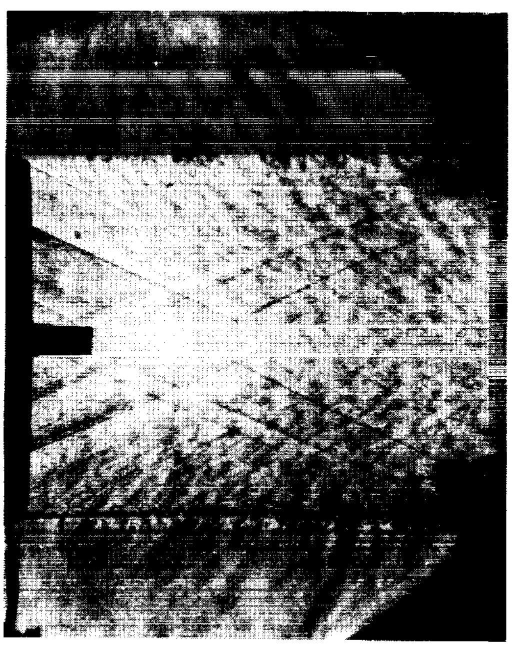

(c) Knife edge normal to flow, flash exposure.

(d) Knife edge normal to flow, time exposure.

L-71-691

Figure 5.- Schlieren photographs for $M_a = 2.50$ and $M_j = 0.91$.

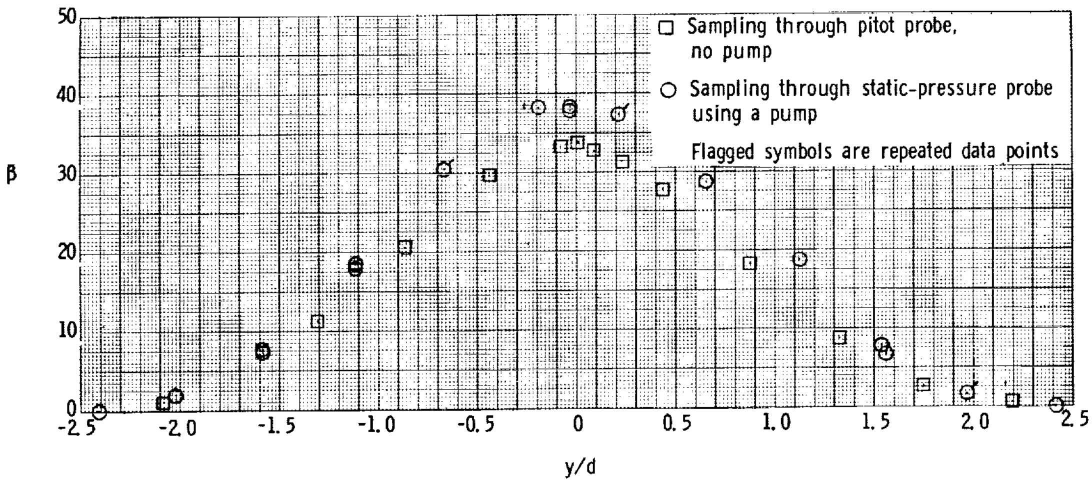

(a) x/d = 42.8.

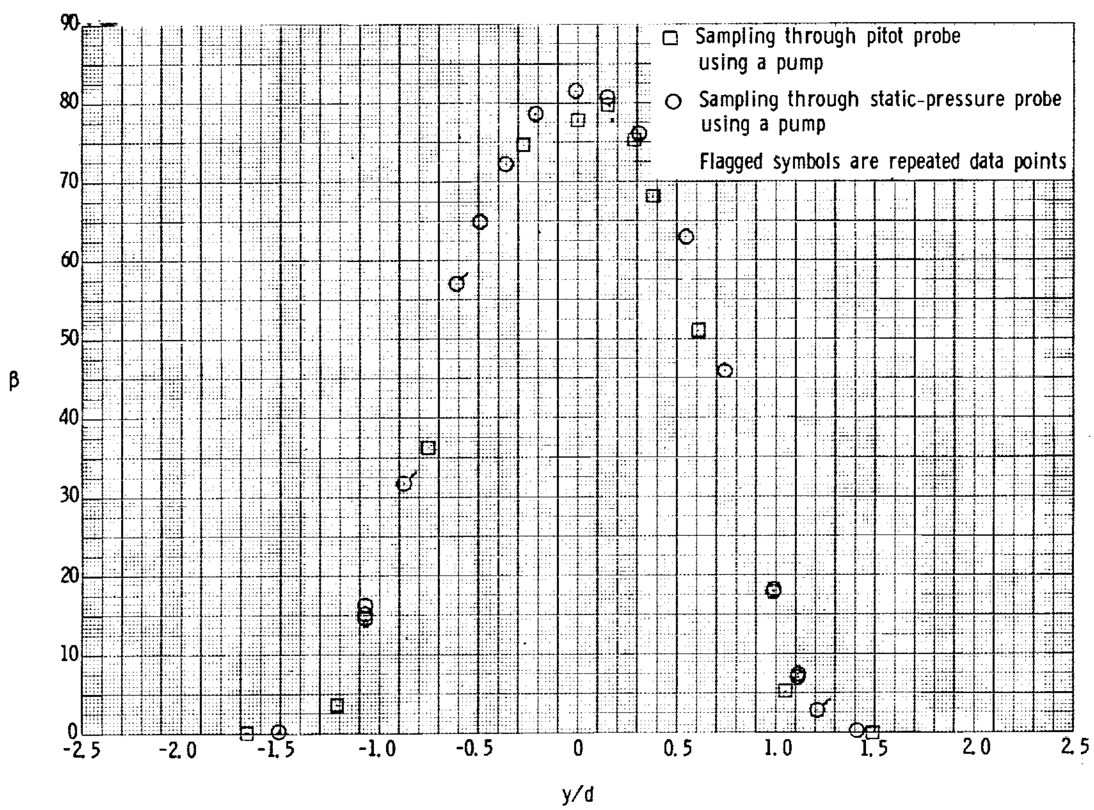

(b) x/d = 15.4.

Figure 6.- Radial distribution of volume fraction of hydrogen for different sampling techniques.

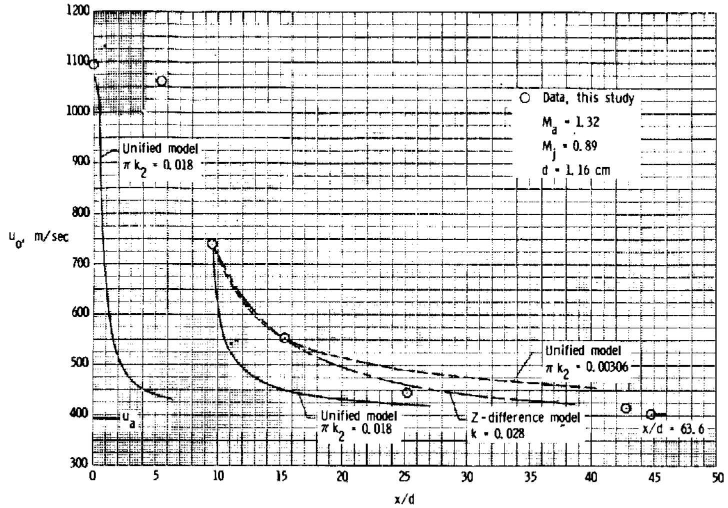

(a) Hydrogen-air mixing for $M_a = 1.32$.

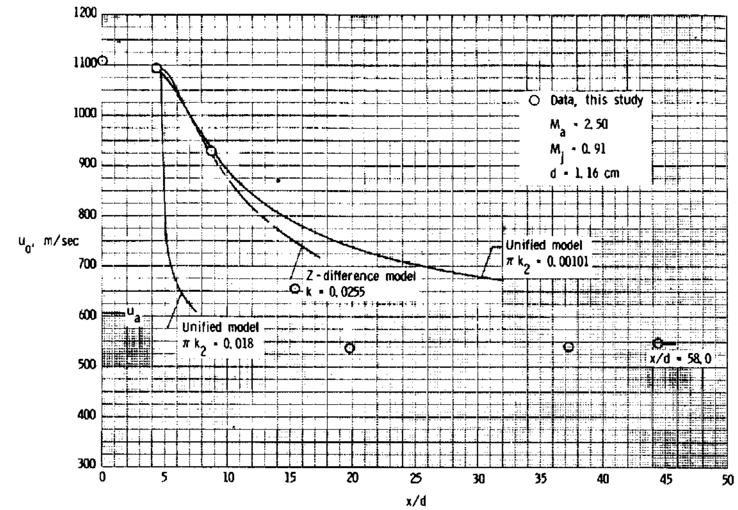

(b) Hydrogen-air mixing for $M_a = 2.50$.

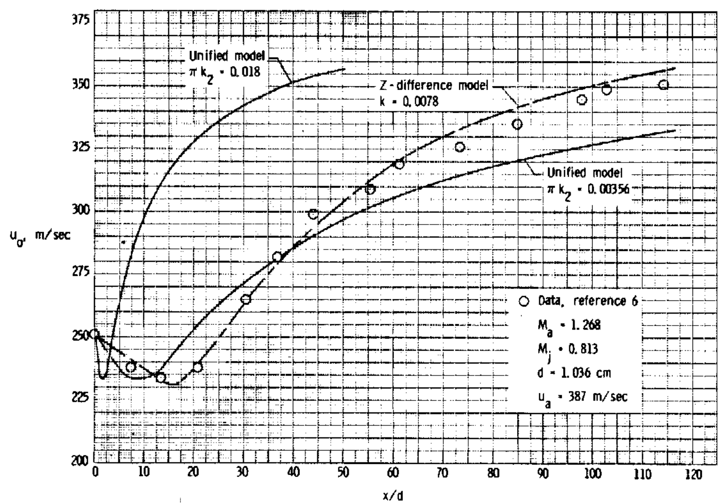

(c) Air-air mixing for $M_a = 1.268$.

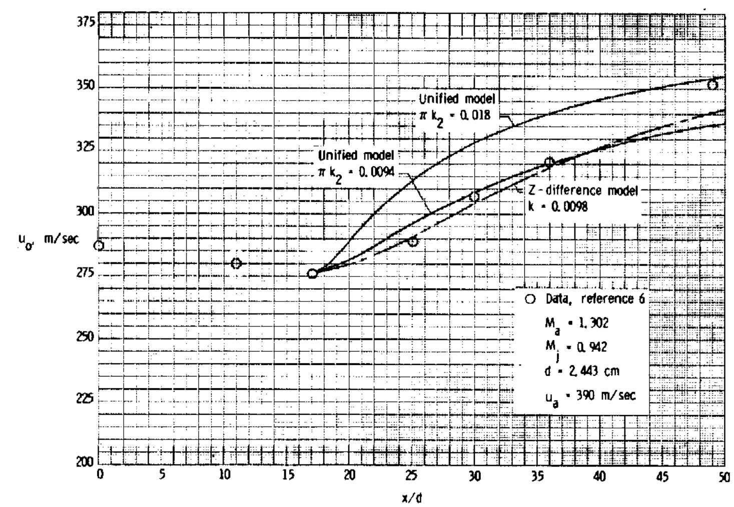

(d) Air-air mixing for $M_a = 1.302$.

Figure 7.- Center-line velocity distributions predicted by unified and Z-difference eddy viscosity models compared with data.

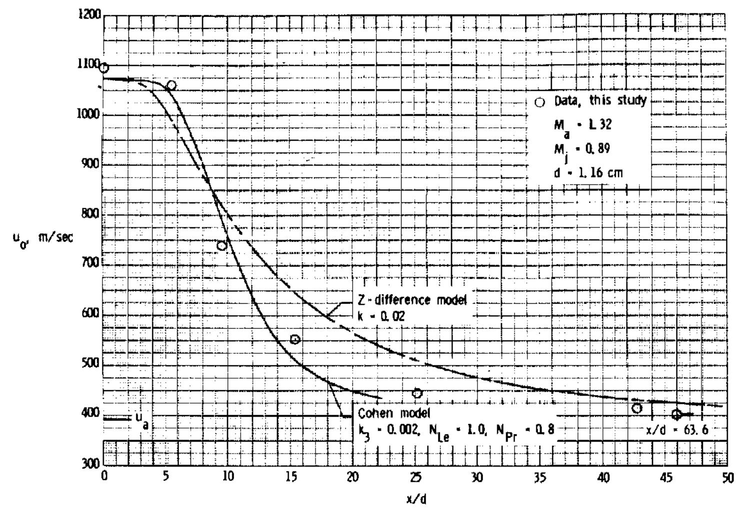

(a) Hydrogen-air mixing for $M_a = 1.32$.

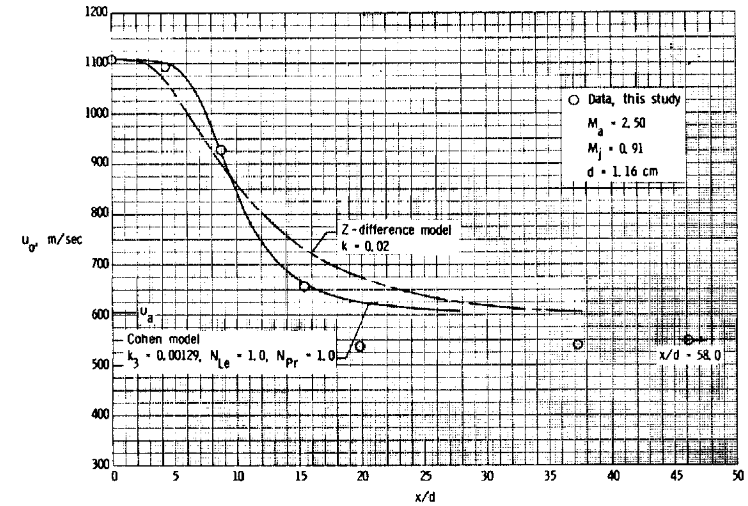

(b) Hydrogen-air mixing for $M_a = 2.50$.

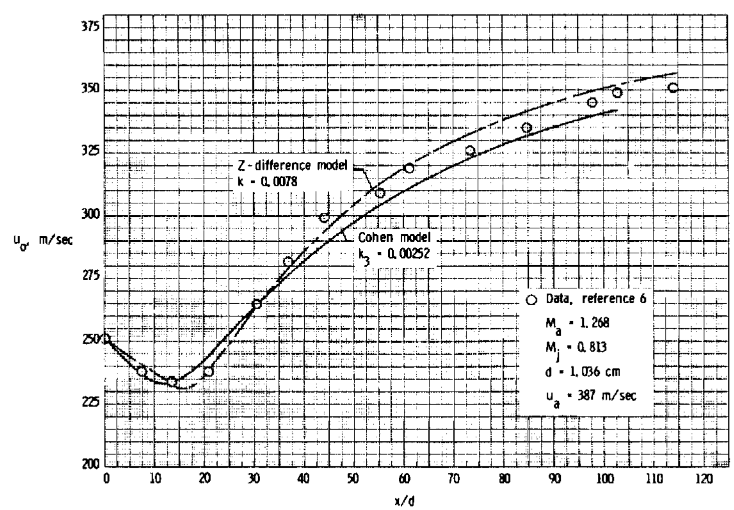

(c) Air-air mixing for $M_a = 1.268$.

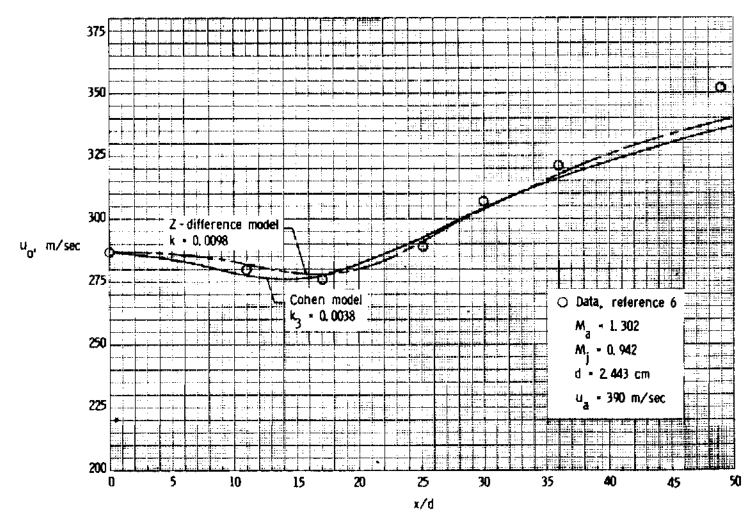

(d) Air-air mixing for $M_a = 1.302$.

Figure 8.- Center-line velocity distributions predicted by Z-difference and Cohen eddy viscosity models compared with data.

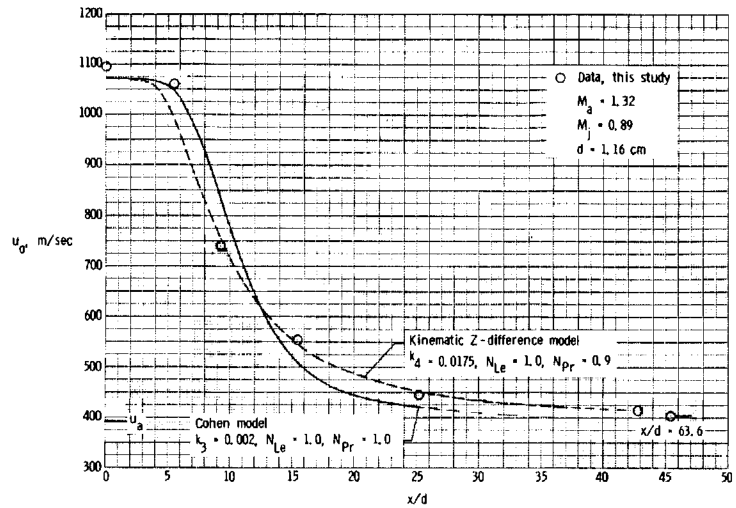

(a) Hydrogen-air mixing for $M_a = 1.32$.

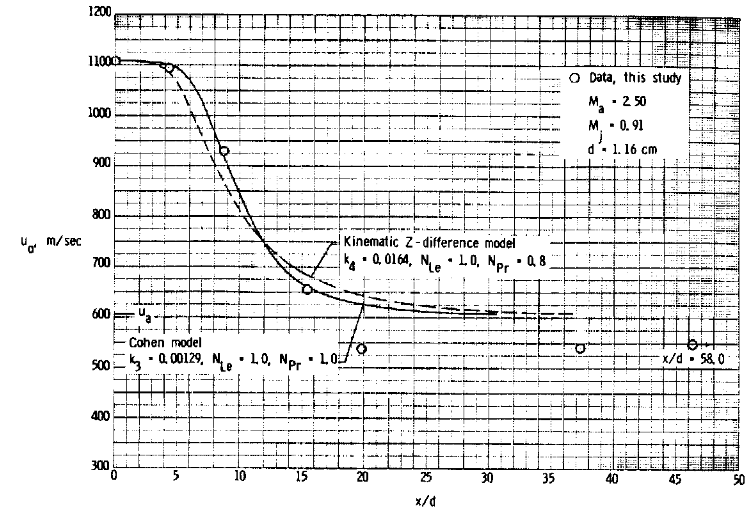

(b) Hydrogen-air mixing for $M_a = 2.50$.

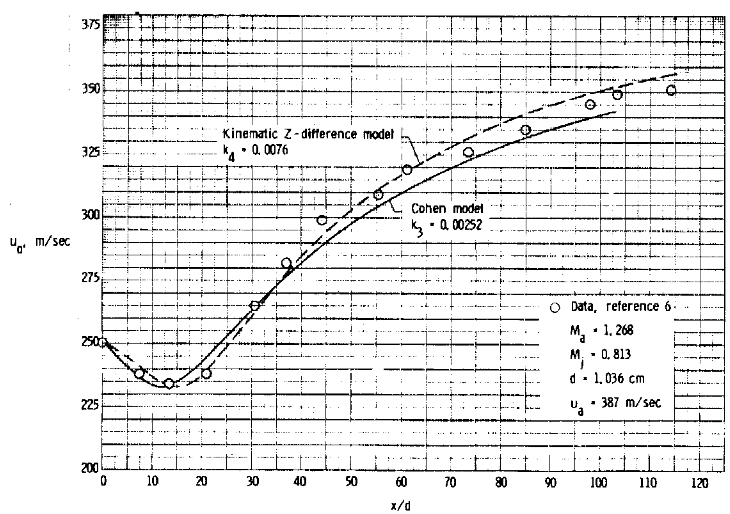

(c) Air-air mixing for $M_a = 1.268$.

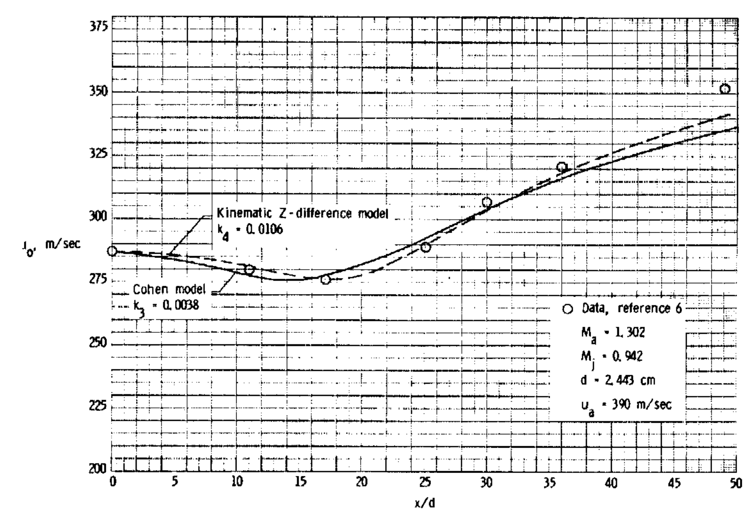

(d) Air-air mixing for $M_a = 1.302$.

Figure 9.- Theoretical center-line velocity distributions as predicted by Cohen and kinematic Z-difference eddy viscosity models compared with data.

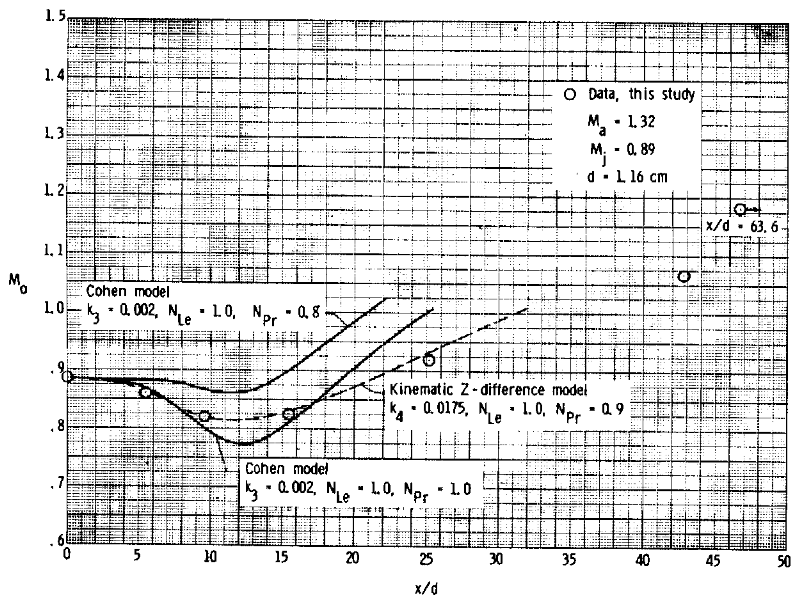

(a) Hydrogen-air mixing; Mach number distribution; M_a = 1.32.

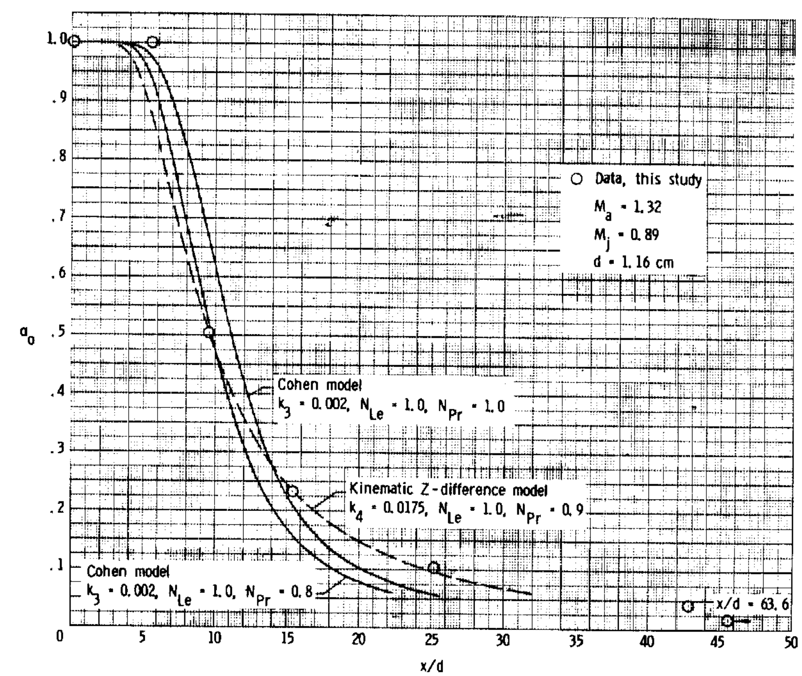

(b) Hydrogen-air mixing; mass fraction of hydrogen distribution; M_a = 1.32.

Figure 10.- Theoretical center-line Mach number and mass fraction of hydrogen distributions predicted by Cohen and kinematic Z-difference eddy viscosity models compared with data.

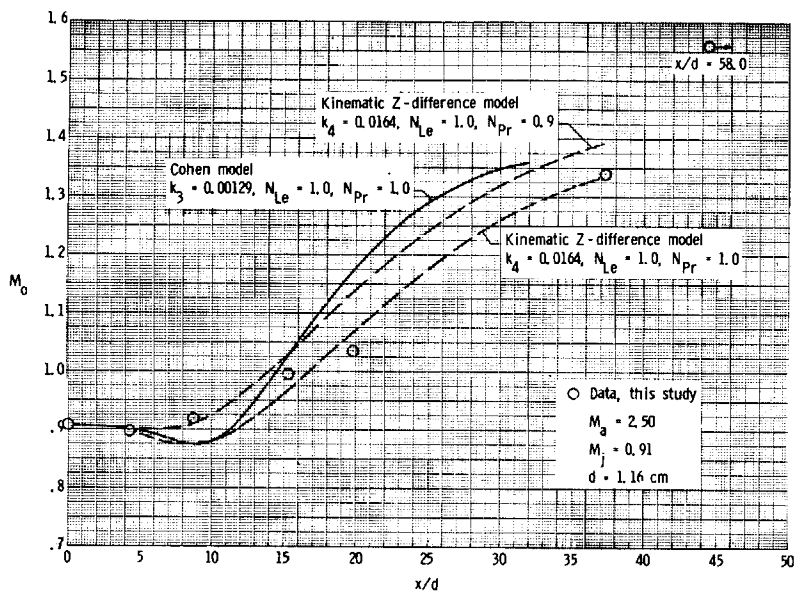

(c) Hydrogen-air mixing; Mach number distribution; $M_a = 2.50$.

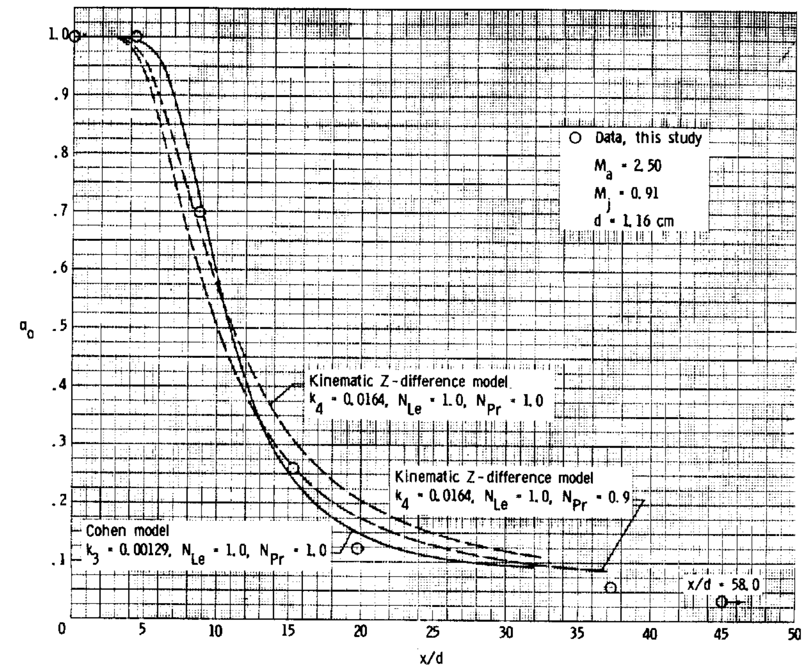

(d) Hydrogen-air mixing; mass fraction of hydrogen distribution; $M_a = 2.50$.

Figure 10.- Concluded.

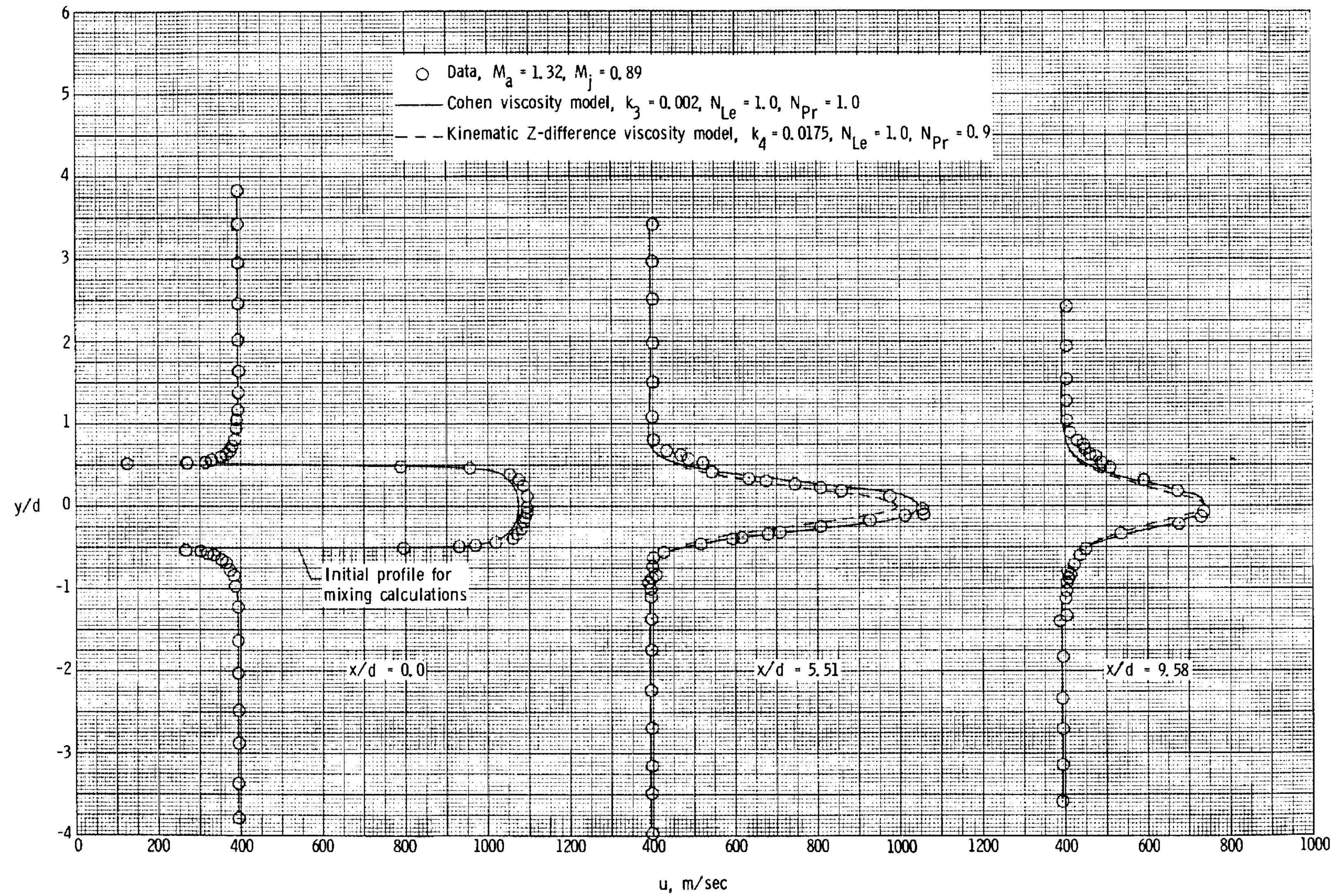

(a) Velocity profiles; x/d = 0.0 to 9.58.

Figure 11.- Hydrogen-air mixing data and correlation for $M_a = 1.32$.

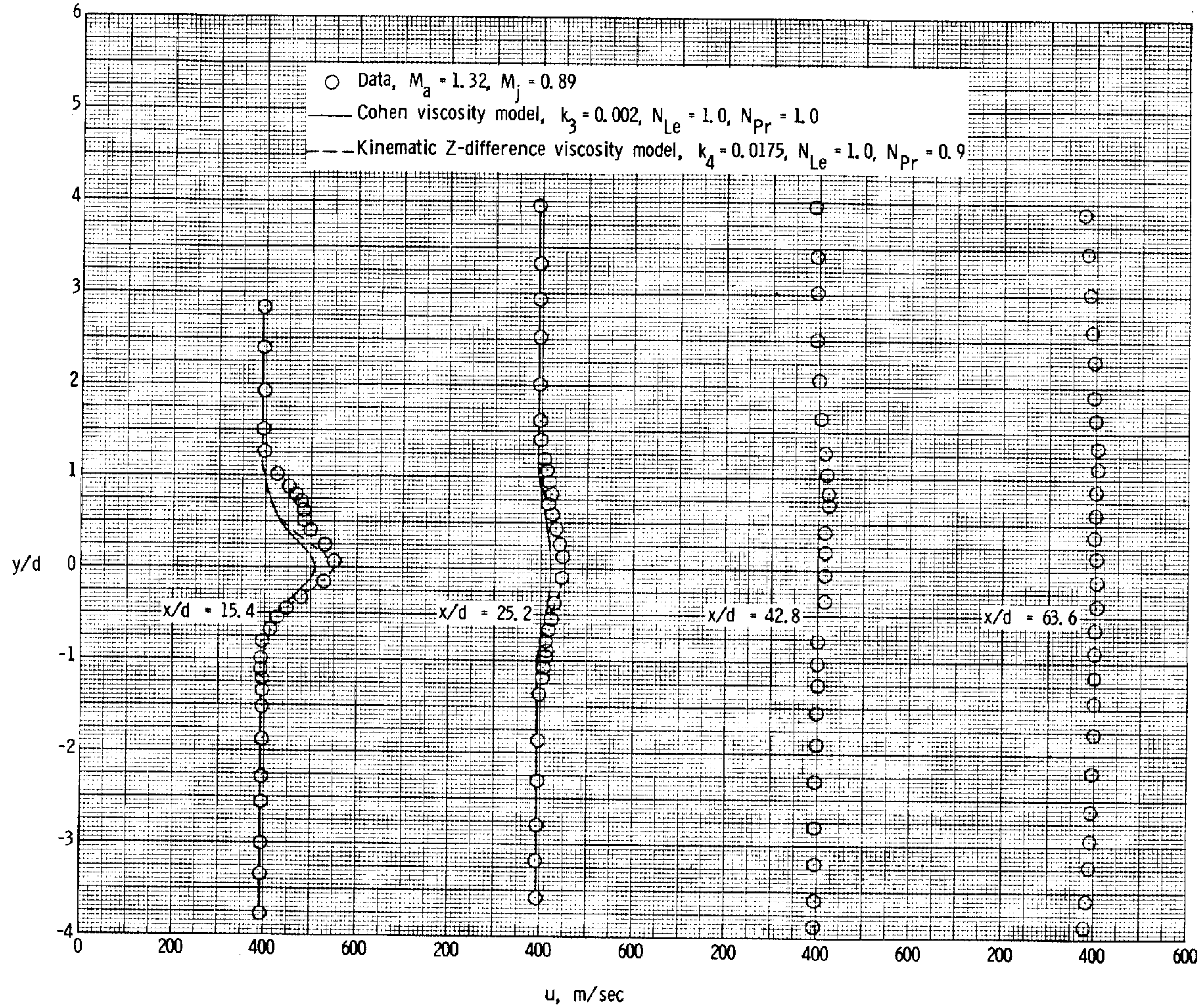

(b) Velocity profiles; x/d = 15.4 to 63.6.

Figure 11.- Continued.

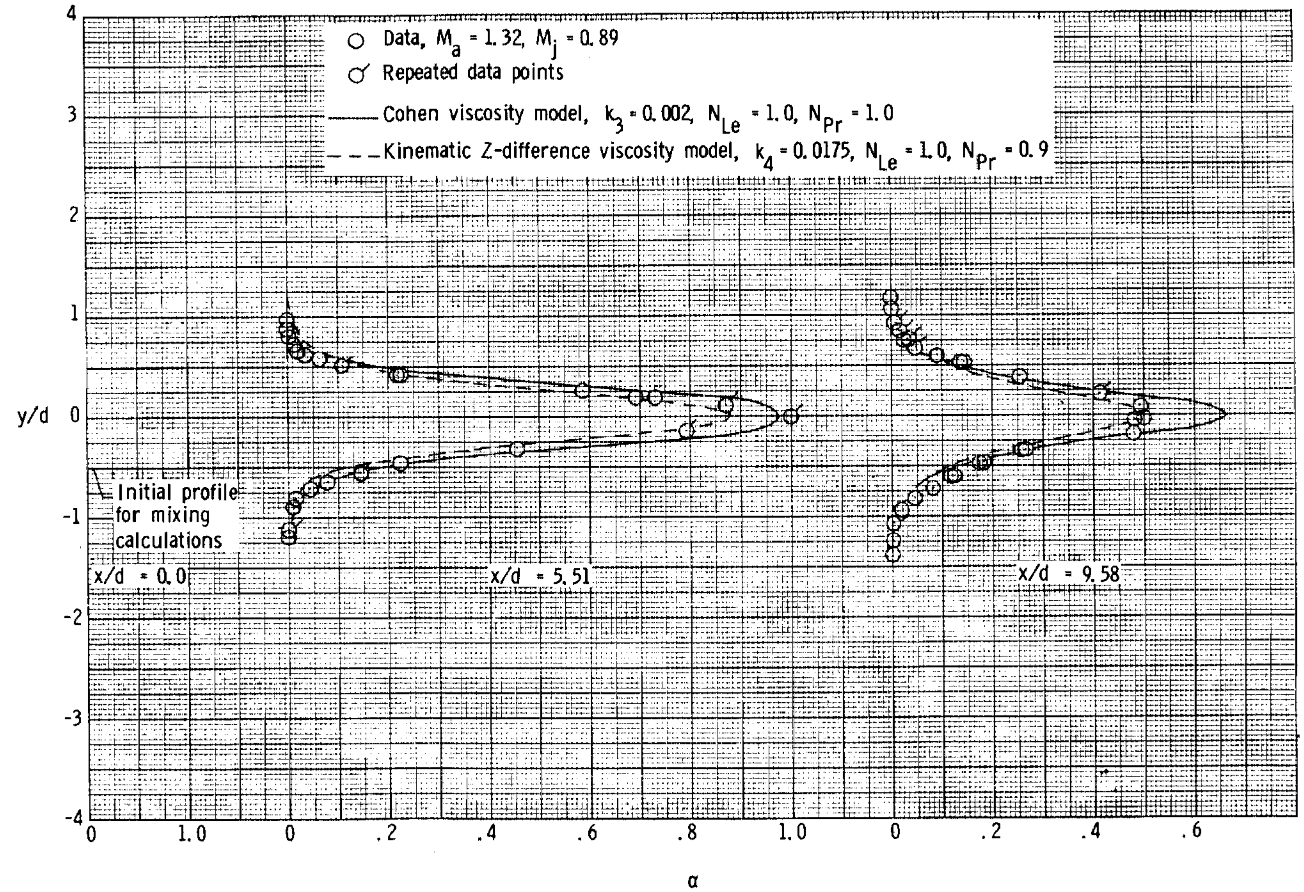

(c) Hydrogen mass fraction profiles; x/d = 0.0 to 9.58.

Figure 11.- Continued.

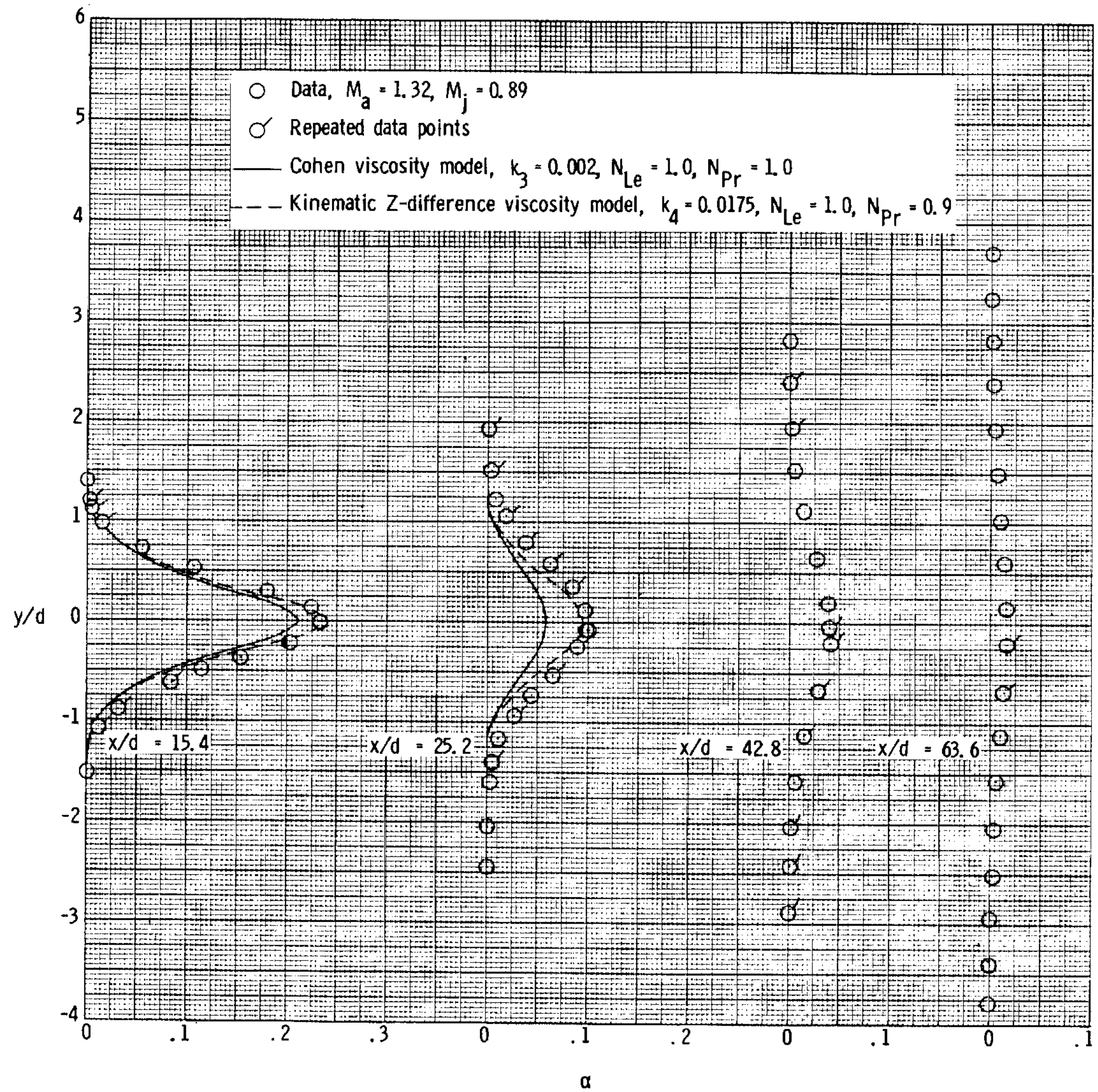

(d) Hydrogen mass fraction profiles; x/d = 15.4 to 63.6.

Figure 11.- Concluded.

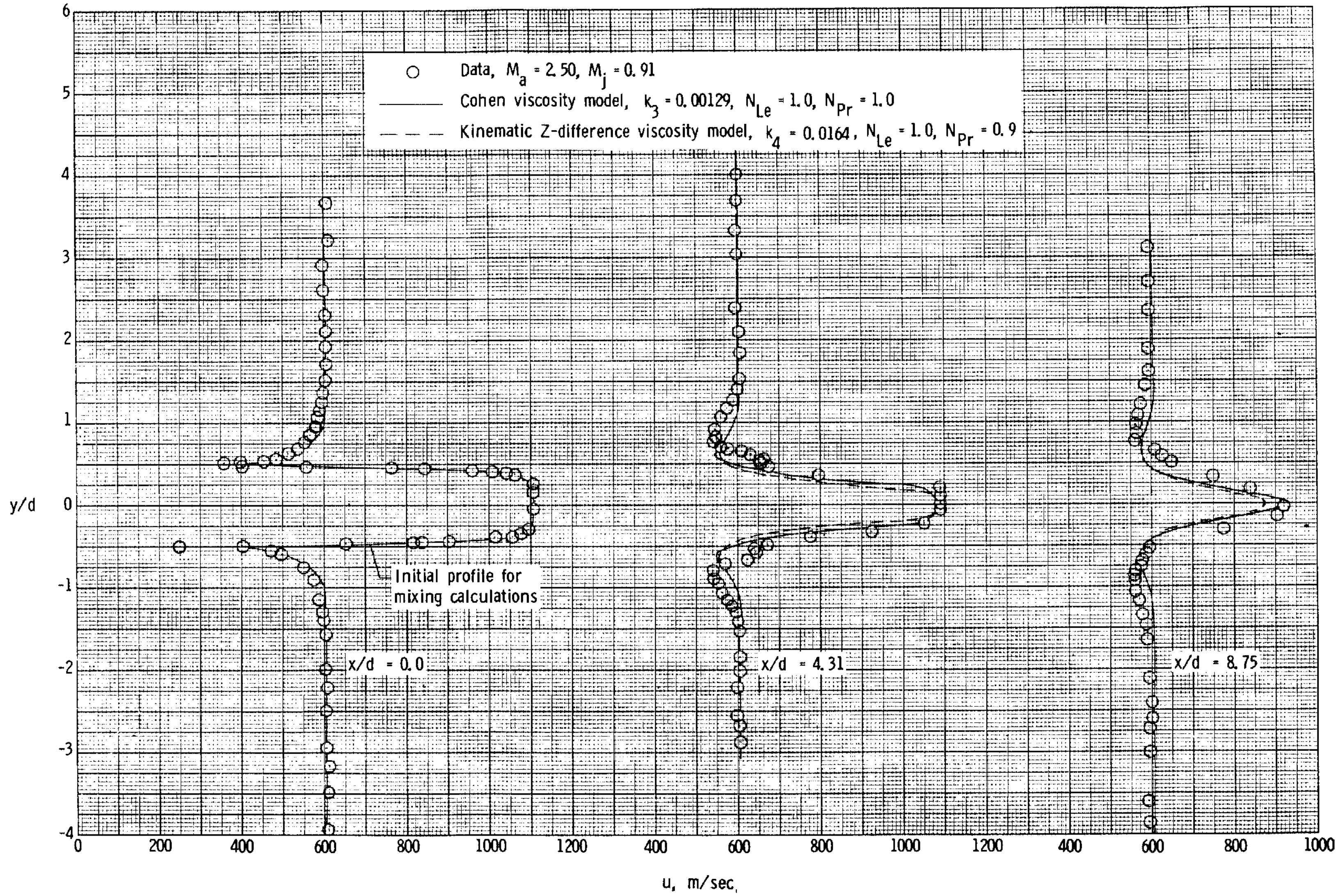

(a) Velocity profiles; x/d = 0.0 to 8.75.

Figure 12.- Hydrogen-air mixing data and correlations for $M_a = 2.50$.

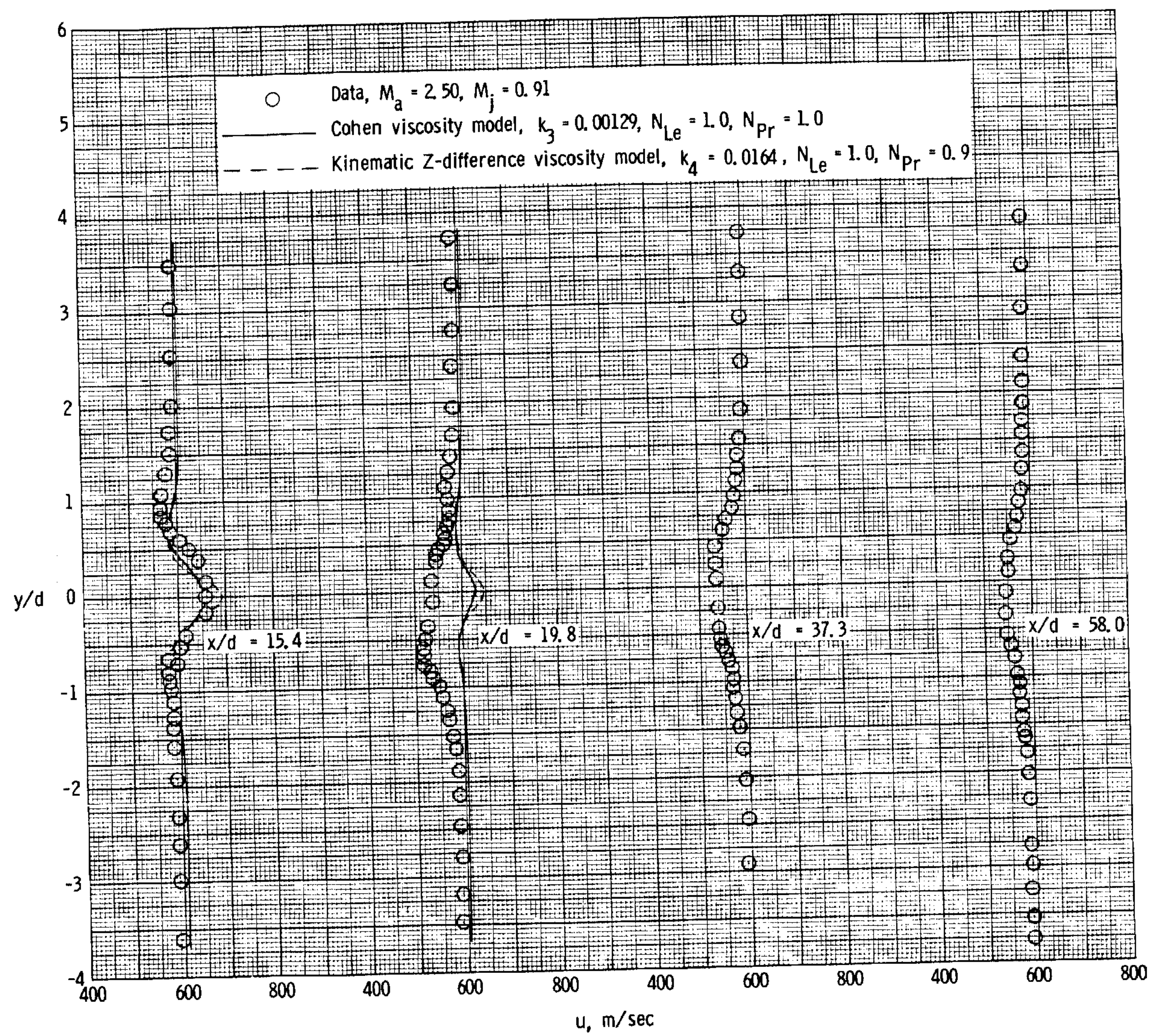

(b) Velocity profiles; x/d = 15.4 to 58.0.

Figure 12.- Continued.

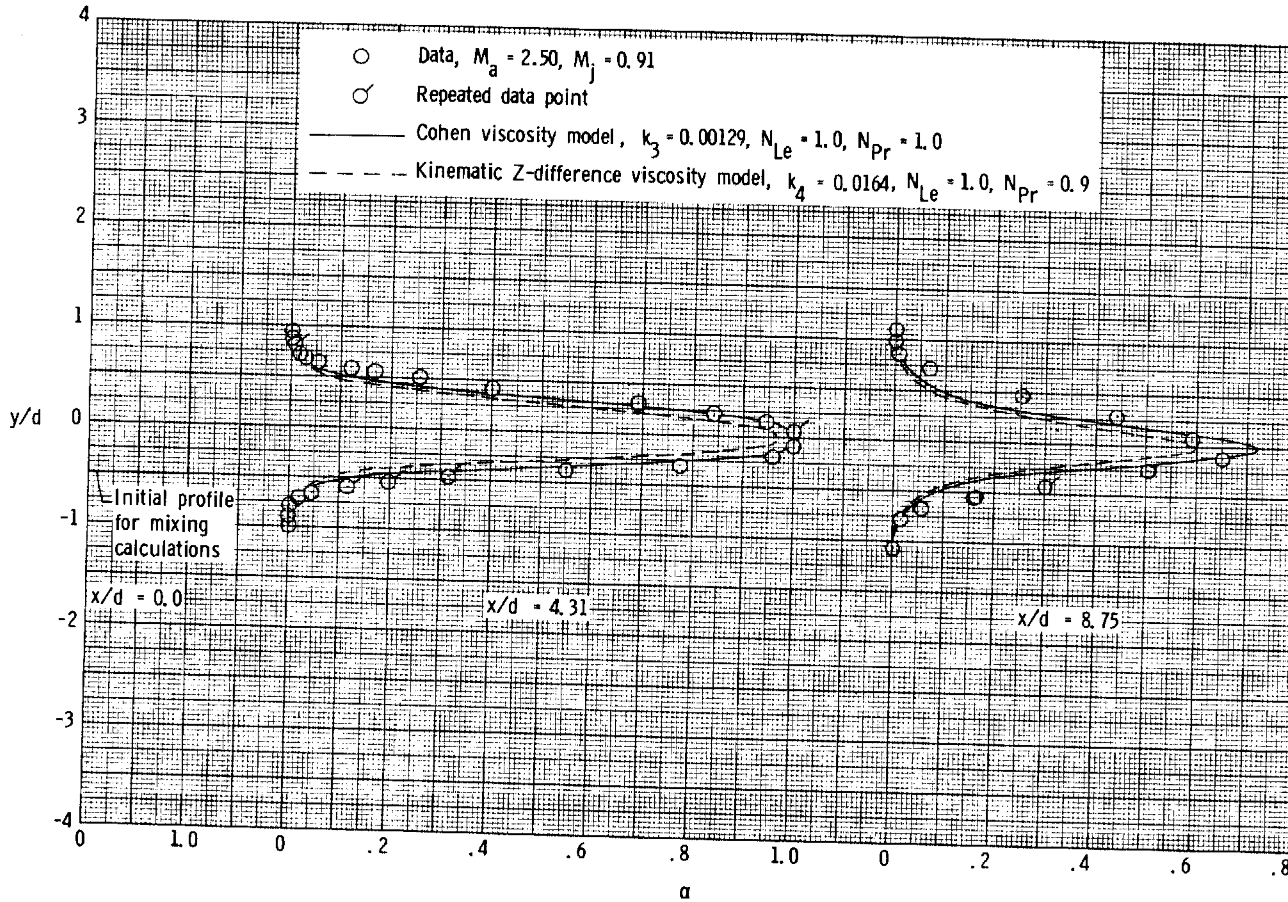

(c) Hydrogen mass fraction profiles; x/d = 0.0 to 8.75.

Figure 12.- Continued.

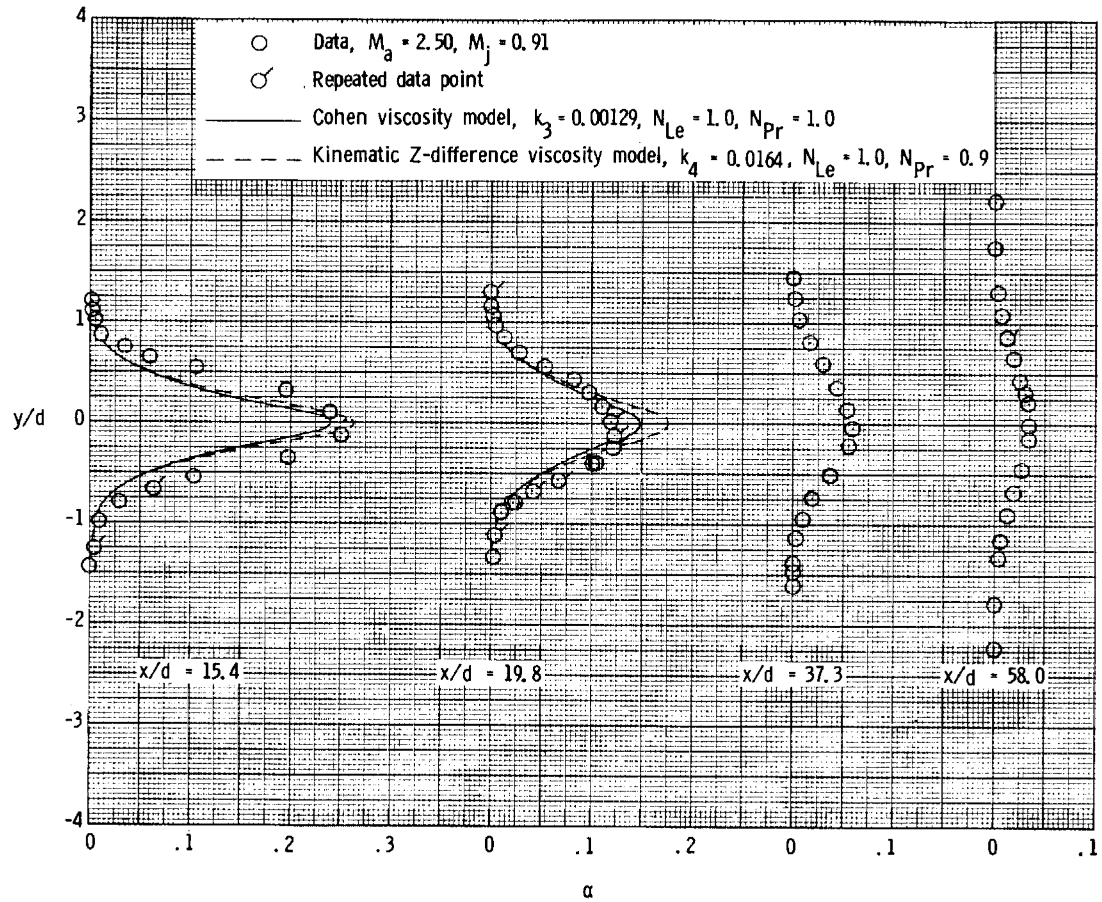

(d) Hydrogen mass fraction profiles; x/d = 15.4 to 58.0.

Figure 12.- Concluded.